이학박사학위논문

Graphene-Based Analytical Platforms for Fluorescence and Raman Spectrometry

형광 및 라만 분석을 위한 그래핀 기반 분석 플랫폼

2017년 2월

서울대학교 대학원

화학부 물리화학전공

이 보 라

Graphene-Based Analytical Platforms for Fluorescence and Raman Spectrometry

지도교수 홍 병 희

이 논문을 이학박사학위논문으로 제출함

2017년 2월

서울대학교 대학원

화학부 물리화학전공

이 보 라

이보라의 박사학위논문을 인준함

2017년 2월

위 원 장 장 두 전 (인)

부 위 원 장 홍 병 희 (인)

위 원 민 달 희 (인)

위 원 김 양 균 (인)

위 원 조 성 표 (인)

Abstract

Graphene-Based Analytical Platforms for Fluorescence and Raman Spectrometry

Bora Lee

Department of Chemistry

The Graduate School

Seoul National University

Chapter 1 describes the general introduction of the thesis. The synthesis methods and properties of graphene are briefly introduced.

One of the fascinating applications of graphene is Graphene-Enhanced Raman Spectroscopy (GERS), which is the phenomenon that the Raman signal of a molecule can be considerably enhanced on graphene, while background fluorescence is quenched due to ultrafast charge carrier mobility of graphene. However, the underlying mechanism of GERS and fluorescence quenching has not been fully understood yet.

In Chapter 2.1, the Raman scattering properties of sandwich structures are investigated, revealing that the enhancement depends on whether the molecular geometries are planar or not. The planar dye molecules between two graphene layers follow the conventional Raman enhancement mechanism induced by the overlap of molecular absorbance and excitation laser wavelengths. On the other hand, abnormal enhancement of Raman signals was observed from graphene-sandwiched nonplanar dye molecules, which is believed to be originated from the

synergistic resonance with new excited energy states created by quantum void space surrounding dye molecules. These results not only provide deeper understanding of the mechanism of GERS but also suggest the graphene-sandwiched resonance Raman Spectroscopy as a more sensitive and robust analytical platform for various chemical and biological studies.

In Chapter 2.2, the single layer graphene by itself is capable of catalyzing the photoreduction of dye molecules, which has been revealed by graphene-enhanced Raman spectroscopy studies. The proposed mechanism involves the electron transfer from graphene to temporarily empty HOMO states of photoexcited dye molecules, which can be interpreted as ultrafast hole transfer from dyes to graphene. It is also confirmed that graphene-encapsulated nitrobenzene dyes show less photoreduction, implying that the ambient hydrogen molecules are the importance source of photoreduction into aniline dyes. The photocatalytic reactivity of graphene would find numerous energy and environmental applications in the future.

In Chapter 3, enhancing the sensitivity and selectivity of graphene-based DNA sensor by surface passivation of graphene will be discussed. Graphene oxide (GO) efficiently quenches the florescence from fluorophore-labeled DNAs, which has been utilized for highly selective and sensitive sensing of DNA hybridization, because the single and double helix DNAs show different binding affinity to GOs. As a result, the introduction of complementary DNAs (c-DNAs) turns on the fluorescence signals as the probe-DNA/c-DNA double helix is detached from the GO surface, while addition of mismatched DNAs (m-DNAs) shows a slight change in the fluorescence signals. However, in actual experiments, it is often observed that the surface of GO is not fully covered with probe-DNAs, and the introduced c-DNAs or m-DNAs bind to the uncovered GO surface rather than interacting with probe-DNAs. This undesired binding considerably degrades the sensitivity and the selectivity of DNA sensing because the

fluorescence intensity change is small with increasing DNA concentration. Thus, the passivation of uncovered GO surface is important to ensure the higher performance of the GO-based DNA sensors.

Keywords : Graphene, Graphene-enhanced Raman spectroscopy, Graphene-sandwich structure, Quantum void space, Photocatalyst, Fluorescence quenching, DNA sensor

Student Number : **2013-22932**

Contents

Abstract i

Contents iv

List of Figures vi

Chapter 1. General Introduction

1.1 The Synthesis of Graphene 1

Mechanical Exfoliation 1

Chemical Exfoliation 2

Chemical Vapor Deposition (CVD) Methods 3

1.2 The Properties of Graphene 6

1.3 References 8

Chapter 2. Graphene Enhanced Raman Spectroscopy and Photocatalysis

2.1 Introduction 13

2.1.1 References 15

2.2 Graphene-Sandwiched Resonance Raman Spectroscopy

2.2.1 Introduction 20

2.2.2 Experimental 22

2.2.3 Results and Discussion 24

2.2.4 Conclusion 29

2.2.5 References 30

2.3 Graphene-Catalyzed Photoreduction of Dye Molecules

2.3.1 Introduction 40
2.3.2 Experimental 42
2.3.3 Results and Discussion 43
2.3.4 Conclusion 48
2.3.5 References 49

Chapter 3. Enhanced DNA Sensing by Surface-Passivated Graphene

3.1 Introduction 63
3.2 Experimental 66
3.3 Results and Discussion 68
3.4 Conclusion 70
3.5 References 71

Appendix

A List of Publication 81
B List of Presentation 82

요약 (국문초록) 83

List of Figures

Chapter 1

Figure 1. Obtaining the various of methods of layered 2D materials (a) mechanical exfoliation, (b) chemically exfoliated graphene oxide, (d) epitaxial growth, (e) chemical vapor deposition method of graphene.

Figure 2. The outstanding properties of graphene for flexible electronics. (a) Mobility as a function of carrier density of a suspended graphene device shows its high electron mobility. (b) Elastic stiffness distribution of graphene film on a silicon oxide cavity. (c) The resistance change of a graphene film transferred onto a polydimethylsiloxane substrate depends on isotropic stretching. (Insets) The resistance change and movement images depend on stretching cycles and stretching direction. (d) Transmittance of partially covered single-layer and bilayer graphene. The inset shows the metal support structure covered with graphene layers.

Chapter 2

Figure 1. Schematic of the electromagnetic and chemical enhancements in SERS.

Figure 2. (a) Schematic illustration of the molecules on graphene and a SiO_2/Si substrate, and the Raman experiments. (b) Schematic illustration and Raman spectra of R6G in water (10 μM) (blue line) and on a graphene film (red line) at 514 nm excitation. (c) Schematic diagram of the UV/ozone oxidized graphene-based chemical enhancement in SERS.

Figure 3. Schematic presentation for resonance change of planar dye. (a) Planar acridine orange of solution state. (b) Adsorbed state of acridine orange on graphene surface with flat configuration. (c) Sandwiched state of acridine orange between two single layered graphene

with flat configuration.

Figure 4. (a) Molecular structure of planar dyes used in the experiments (b) Absorbance of bulk sample of three planar dyes of acridine orange (AO), nile red (NR), and methylene blue (MB) dispersed in ethanol. Two vertical lines are excitation laser wavelengths of 514.5 and 633 nm used for resonance Raman measurements. (c) Absorbance spectra of methylene blue at adsorbed state on graphene surface (black line) and sandwiched state between graphene (red line) (d) Raman spectra of MB dye measured at 633 nm for adsorbed state on graphene surface (black, GERS substrate) and sandwiched state between graphene (red, our sandwich substrate). See the supporting information for the Raman spectra of AO and NR. (e) Baseline-subtracted Raman intensity of the peak denoted as asterisk in spectra of (d). G and 2D peak of graphene are clearly shown at ~1590 and ~2645 cm^{-1}, respectively. Scale bar stands for 1000 Raman counts in our experimental condition.

Figure 5. Raman spectra of planar dye of Acridine Orange (AO) and Nile Red (NR) adsorbed on graphene surface (black) and sandwiched between two graphene sheets (red).

Figure 6. (a) Molecular structure of nonplanar dyes used in the experiments (b) Absorbance of five nonplanar dyes of rhodamine 123 (Rh-123), rhodamine 6G (R6G), rhodamine B (Rh-B), coomassie brilliant blue g250 (CB-g250), and xylene cyanol ff (XC-ff) dispersed in ethanol. Two vertical lines are excitation laser wavelengths of 514.5 and 633 nm used for resonance Raman measurements. (c) Absorbance spectra of R6G at adsorbed state on graphene surface (black line) and sandwiched state between graphene (red line) (d) Raman spectra of nonplanar dye measured at 514.5 nm from adsorbed state on graphene surface (black, GERS substrate) and sandwiched state between graphene (red, our sandwich substrate). (c) Baseline-subtracted Raman intensity of the dye peak denoted as asterisk in spectra of (b). G and 2D peak of graphene are clearly shown at ~1589 and ~2690 cm^{-1}, respectively. Scale bar stands for 1000

Raman counts.

Figure 7. Raman spectra of nonplanar dye of rhodamine 123 (Rh-123), rhodamine B (Rh-B), coomassie brilliant blue g250 (CB-g250), and xylene cyanol ff (XC-ff) adsorbed on graphene surface(black) and sandwiched between two graphene sheets (red).

Figure 8. Schematic representation of mechanism of Raman signal enhancement of nonplanar dye observed in Figure 6. (a) Encapsulation of nonplanar dye (R6G) between graphene. (b) Comparison of background intensity of planar dye and nonplanar dye extracted from the Raman spectra in Figure 4 and Figure 6 (baseline Raman scattering intensity at the position of peak denoted as asterisk).

Figure 9. Scheme for comparing the fluorescence quenching efficiency and Raman scattering intensity between the case of planar dye and nonplanar dye.

Figure 10. Raman intensity variation of nonplanar dye (XC-ff, xylene cyanol-ff), graphene G and graphene 2D peaks according to the structure. It shows that all Raman signals (dye, G, 2D) in 'dye-**between**-two sheets of graphene' structure are enhanced compared to the 'dye-**on**-two sheets of graphene' structure.

Figure 11. DFT calculation (B3LYP 6-31G(d,p) level, GAUSSIAN 03W) results of Raman spectra of rhodamine 6G according to the change of dihedral angel between xanthene and phenyl ring planes. As the dihedral angle increases, Raman intensity has not been changed significantly until 40 degree. Rather, new vibrational bands start to appear from the angle of 50 degree, which was not observed in our experimental data in Figure 6d.

Figure 12. a) Schematic diagram of the graphene-catalyzed photoreduction of DR1. (b) Molecular structures of nitro/amino-DR1.

Figure 13. Raman spectra of DR1 on graphene (red) and without graphene (black).

Figure 14. (a) Time evolution of Raman spectra of DR1 adsorbed on a single layer graphene. Laser excitation wavelength, 514.5 nm. (b) Simulated Raman spectra of trans-NO_2-DR1, trans-NH_2-DR1, and cis-NO_2-DR1 calculated by a DFT method (B3LYP- 6-31G (d,p)).

Figure 15. Normal Raman Spectra of nitro-DR1, amino-DR1 (after exposure to laser for 120 sec) and 4'-amino-DAB. (Inset) The molecule structure of 4'-amino-DAB.

Figure 16. Photoreduction rate of DR1 without graphene compared to that on graphene.

Figure 17. Time evolution of Raman Spectra of DR1 adsorbed on graphene by defocused laser.

Figure 18. (a) Change in Raman spectra of DR1 on graphene with increasing laser irradiation time. The inset shows the magnified plots of G and 2D band peaks related to graphene. Time dependent change in Raman G and 2D peak positions and full width at half maximum (FWHM) are shown in (b) and (c), respectively.

Figure 19. Graphene-encapsulated nitrobenzene dyes show less photoreduction, implying that the ambient hydrogen molecules are the importance source of photoreduction.

Figure 20. Schematic diagram of the graphene Fermi level variation which was treated UV/ozone.

Figure 21. XPS spectra of pristine graphene (a) and oxidized graphene by treating ozone for 10 minutes. (c) shows the evolution of the Raman spectra of the graphene surface as a function of UV/ozone exposure time from 0 to 10 min.

Figure 22. Raman spectra of DR1 adsorbed onto pristine graphene (0 min) and ozone-treated graphene for 5 and 10 min.

Figure 23. Photoreduction rate of DR1 adsorbed onto pristine graphene and ozone-treated graphene for 5 and 10 min.

Chapter 3

Figure 1. Chemical structure of DNA. Dotted lines shown are hydrogen bonds between the bases.

Figure 2. (a) Scheme of FAM-labeled DNA adsorption and desorption on GO. Fluorescence is quenched upon adsorption. Desorption can be achieved by adding the c-DNA (reaction 1), DNA exchange with the same DNA (reaction 2), or increasing temperature (reaction 3). (b) Schematics of covalently linked probes with GO. The fluorescence properties of the GO samples containing only covalently attached DNAs were analyzed. (c) Displacement mechanism of hybridization between a probe DNA adsorbed by GO and its cDNA (target DNA). The oxygenated groups and defeats on GO are omitted. In the case, the probe DNA with a fluorophore label is preadsorbed and the cDNA is added afterward. The tendency of GO adsorbing dsDNA is lower than that of the adsorption of ssDNA.

Figure 3. Schematic presentation of the DNA-GO complex through passivation method.

Figure 4. Fluorescence intensity of probe DNA with FAM as the volume of GO and reference (only GO, buffer).

Figure 5. The fluorescence spectrum of dye-labeled DNA-GO complex (black line) and the mixture of DNA-GO complex and passivation DNA (red line). When passivation DNA was added, fluorescence was revealed.

Figure 6. The relative fluorescence spectra at various concentrations of complementary DNA (a, b) or mismatched DNA (c, d). (a) and (c) are not passivated on surface of GO, while (b) and (d) are passivated on surface of GO.

Figure 7. The relative fluorescence of dye-labeled probe DNA at 517nm with log value of concentration of c/m-DNA. It is replotted data in figure 6. It is indicated that the recovery of

fluorescence without (a) and with (b) passivation on surface of graphene oxide.

Chapter 1. General Introduction

Graphene, a single sheet of sp^2-bonded carbon atoms in a 2D honey-comb structure, possesses unique optical, thermal, electronic and mechanical properties. Intrinsic graphene is characterized as a semi-metal or zero-gap semiconductor and its unique electronic properties produce an unexpectedly high opacity for an atomic monolayer. Electrical properties has a remarkably high electron mobility at room temperature.

Furthermore, since graphene shows very high surface area, good biocompatibility and high adsorption capacity, Graphene and its derivatives can be used as valuable substrates in wide range of applications.

1.1 The Synthesis of Graphene

Mechanical Exfoliation

Exfoliation, elaborated mainly by the Manchester group, is basically a repeated peeling process.[1] It is possible to produce graphene from a high purity graphite because graphite is stacked layers of many graphene sheets, bonded together by weak van der Waals force of about 2 eV/nm^2.[2] Although the first attempt was by rubbing micro-fabricated arrays of graphite micropillars, they do not allow thinning the graphite below a few nanometers.

Since Novoselov and Geim obtained graphene using common adhesive tape, this has generally involved using either an adhesive tape to attach to the surface of bulk and using force to peel off the tape plus the sheets of graphite attached or by rubbing the surface of bulk against another material to slide off layered 2D material sheets from the bulk.

Many routes have been demonstrated for exfoliation, including micromechanical exfoliation,[1-3] and intercalation steps.[4,5] The ease of production and low cost make exfoliation of layered graphite the most popular route to prepare graphene. In addition, mechanical exfoliation method has no special equipment needed and provides high crystalline structure of graphene. However, the main drawback of this technique is that it does not provide sufficient output yield for many applications. It is not suitable for large-scale production because it is serendipitous, labor intensive. Moreover, it can leave glue residues on the sample, which have since then been shown to limit the carrier mobility. [6]

Chemical Exfoliation

The idea of exfoliating a layer of graphene from graphite to obtain graphene quickly expanded to other variation such as chemical exfoliation. It utilizes strong acids and oxidants to produce graphene oxide (GO) from graphite. Graphene oxide is the name given to graphene that has been oxidized and as such the pristine nature of the graphene lattice disrupted. The oxidization of graphite has been the subject of investigation since at least the mid-19th century.[7,8] One of the first reports was by Brodie (1860) where graphite was treated with potassium chlorate ($KClO_3$) and fuming nitric acid (HNO_3). Staudenmaier (1898) later improved this approach for oxidizing graphite by slowly assed the potassium chlorate over the course of a week to a solution containing concentrated sulphuric acid, concentrated nitric acid (63%) and graphite. However, needing a 10:1 mass ratio of potassium chlorate to graphite, researchers found this method dangerous due to possibility of explosion and time-consuming. More than 56 years later Hummers and Offeman (1958) reported an alternative 'safer' method known as the Hummers method, which involved a water-free mixture of concentrated sulphuric acid, sodium nitrate, and potassium permanganate. Temperatures of only 45℃ were required and the entire reaction took only 2 hours to complete.

All three methods involve oxidation of graphite to various levels. Graphite salts made by intercalating graphite with strong acids such as H_2SO_4, HNO_3 or $HClO_4$ have also been used as precursors for the subsequent oxidation to GO. Graphene oxide disperse well in water due to the negative surface charges on the sheets that arise from the phenols and carboxylic acid groups that decorate graphene oxide and keep it from reaggregating.[9] The hydrophilic nature of graphene oxide means that water molecules easily intercalate graphite oxide, leading to variable inter-sheet separations ranging from 0.6 nm to 1.2 nm.[10]

For many years there was uncertainty regarding the specific atomic structure of graphite oxide and subsequently graphene oxide. In many of the graphite oxide structure studies, solid-state NMR was used to provide insights, however, the low nature abundance of ^{13}C leads to relatively poor signal to noise ratio. Cai *et al*. overcome this problem by using synthetic ^{13}C labelled graphite to prepare graphene oxide.[11]

Chemical Vapor Deposition (CVD) Methods

The fabrication of graphene over metals by chemical vapor deposition is one of the most popular synthesis routes. The reasons for this are various and include the potential to scale-up fabrication, the technique is already well established in industrial settings and it is easy to set-up in research laboratories amongst other attractive traits. CVD grown graphene over metals can also be established in over large areas and this is important for applications, for example, transparent conducting electrodes for solar cells, where a contiguous covering of graphene is required. This is fundamentally different to exfoliation routes that result in graphene flakes scattered randomly over a substrate.

The chemical vapor depositing of sp^2 carbon entails passing a carbon feedstock over the surface of a catalyst substrate (e.g. transition metal) at elevated temperatures. The catalyst then

catalytically decomposes the feedstock to provide a supply of carbon. The catalytic potential of transition metals is well established and is argued to arise from partially filled d orbitals or by the formation of intermediate compounds which can absorb and activate the reacting medium. In essence, the metals provide low energy pathways for reactions by changing oxidation states easily or through the formation of intermediates. Once the feedstock has decomposed and provided a source of carbon, the carbon can be absorbed by the metal and then later precipitate out to form graphene as for example Ni and Co, or if carbon solubility is limited, then sp^2-carbon formation can occur as a surface process as for example is the case for Cu.

Intensive early studies using nickel soon revealed a fundamental limitation with this catalyst, namely that single and few layer graphene is obtained over tens of microns and is not homogeneous across the substrate surface. In other words, control over the number of layers is limited. This is argued to occur because Ni has a large carbon solubility.[12] Above 800 °C, carbon and nickel form a solid solution. The solubility of carbon decreases below 800°C so that upon cooling, carbon diffuses out of the Ni. In short, carbon segregation is rapid within Ni grains and heterogeneous at grain boundaries. This means the number of graphene layers that form at grain boundaries exceeds that forming over Ni grains and leads to a variation in the number of graphene layers forming on the surface. To some degree this can be alleviated by using single crystalline Ni, however whilst this is attractive for producing graphene for fundamental studies, it is limited in practical terms for large area and cost.

Copper has a low carbon solubility at high temperature (0.008 weight% at 1084 °C).[13] The interest in copper as a substrate stems from its potential to catalyze various carbon allotropes such as graphite,[14] diamond,[15] and carbon nanotubes.[16] Unlike most substrate with high carbon solubility at elevated temperature, substrates with low carbon solubility allow more facile

single graphene formation over large areas, for example on Cu foil. Graphene formation over ruthenium has also been demonstrated. Ru has a carbon intermediate carbon solubility at high temperature. With Ru implementing a gradual decrease in temperature enables uniform graphene nucleation and growth.[14]

A great advantage of Cu is that it can be grown over huge areas. Bae et al. demonstrated this beautifully in a roll to roll process for the production of predominantly 30-inch graphene film.[17] The films were found to have a sheet resistance of around 150 Ω/square with 97.4% optical transmittance and exhibit half-integer quantum hall effect which highlights the high quality of the material making it suitable for transparent electrode fabrication on an industrial scale.

1.2 The Properties of Graphene

As above mentioned, graphene has a unique band structure that results in many attractive electronic properties, such as a 10–100-times-higher carrier mobility than Si. In 2008, Kim's group showed that single-layer graphene prepared by using the mechanical exfoliation method exhibited carrier mobility in excess of 200,000 cm2/(V·s) at room.[18] By fabricating a suspended graphene channel, they were able to minimize substrate-induced scattering and to obtain essentially ballistic charge transport at millimeter length scales at room temperature.

Lee et al.[19] reported that single-layer graphene is mechanically very strong. They showed that when a graphene sheet suspended across 1.0–1.5-μm cavities in a SiO_2 film was deflected using an AFM tip, the graphene sheet stayed intact and exhibited a Young's modulus of 1 TPa and a large spring constant (1–5 N/m). The excellent mechanical properties of graphene have also been investigated by measuring the electrical resistance on stretching, and as shown in Figure 2c, the resistance shows little variation with strain.[20] This combination of large strain capability and small changes in resistance is necessary for the operation durability of a flexible and stretchable device.

Presently, ITO is widely used as a transparent conductor for optoelectronic devices. However, ITO has poor mechanical properties; it tends to crack easily or shows defects when strained. For these reasons, the use of graphene has been widely investigated in recent years as a transparent conductor for optoelectronic and photonic applications because of its combination of electrical, mechanical, and optical properties. The optical properties of graphene result in high opacity for an atomic monolayer. The transmittance of graphene decreases approximately 2.3% with each layer as the number of graphene layers increases.[21] Furthermore, graphene films transferred onto flexible polyethylene terephthalate (PET) and stretchable PDMS substrates maintain their high transparency and flexible properties.[22]

The adsorption of various molecules on the graphene surface is possible because of graphene's hydrophobic surface, which is similar to that of carbon nanotubes (CNTs). Also, the conductivity and doping types can be modified by chemical treatment. There are now numerous reports of doping methods such as modification of the substrate surface with self-assembled monolayers; sp3 functionalization of carbon with H, F, or Cl; atomic substitution with N; and surface treatment of graphene by using certain molecules or acidic solutions.[23-26]

1.3 References

1. Novoselov, K. S.; Geim, A. K.; Morozov, S. V.; Jiang, D.; Zhang, Y.; Dubonos, S. V.; Grigorieva, I. V.; Firsov, A. A., Electric Field Effect in Atomically Thin Carbon Films. *Science* **2004,** *306* (5696), 666-669.
2. Zhang, Y. B.; Small, J. P.; Pontius, W. V.; Kim P., Fabrication and electric-field-dependent transport measurements of mesoscopic graphite devices. *Appl. Phys. Lett.* **2005**, 86 (7), 073104.
3. RadisavljevicB; RadenovicA; BrivioJ; GiacomettiV; KisA, Single-layer MoS_2 transistors. *Nat. Nanotechnol.* **2011,** *6* (3), 147-150.
4. Zhu, J., Graphene production: New solutions to a new problem. *Nat. Nanotechnol.* **2008,** *3* (9), 528-529.
5. Eda, G.; Yamaguchi, H.; Voiry, D.; Fujita, T.; Chen, M.; Chhowalla, M., Photoluminescence from Chemically Exfoliated MoS_2. *Nano Lett.* **2011,** *11* (12), 5111-5116.
6. Soldano, C.; Mahmood, A.; Dujardin, E., Production, properties and potential of graphene. *Carbon* **2010**, 48, 2127-2150.
7. Brodie, B., Sur le poids atomique du graphite. *Ann. Chim. Phys* **1860,** *59* (466), e472.
8. Hummers Jr, W. S.; Offeman, R. E., Preparation of graphitic oxide. *J. Am. Chem. Soc.* **1958,** *80* (6), 1339-1339.
9. He, H.; Klinowski, J.; Forster, M.; Lerf, A., A new structural model for graphite oxide. *Chem. Phys. Lett.* **1998,** *287* (1), 53-56.
10. Buchsteiner, A.; Lerf, A.; Pieper, J., Water dynamics in graphite oxide investigated with neutron scattering. *J. Phys. Chem. B* **2006,** *110* (45), 22328-22338.
11. Cai, W.; Piner, R. D.; Stadermann, F. J.; Park, S.; Shaibat, M. A.; Ishii, Y.; Yang, D.;

Velamakanni, A.; An, S. J.; Stoller, M., Synthesis and solid-state NMR structural characterization of 13C-labeled graphite oxide. *Science* **2008,** *321* (5897), 1815-1817.

12. Mattevi, C.; Kim, H.; Chhowalla, M., A review of chemical vapour deposition of graphene on copper. *J. Mater. Chem.* **2011,** *21* (10), 3324-3334.
13. Oshima, C.; Nagashima, A., Ultra-thin epitaxial films of graphite and hexagonal boron nitride on solid surfaces. *J. Phys.: Condens. Matter* **1997,** *9* (1), 1.
14. Ong, T.; Xiong, F.; Chang, R.; White, C., Nucleation and growth of diamond on carbon-implanted single crystal copper surfaces. *J. Mater. Res.* **1992,** *7* (09), 2429-2439.
15. Constant, L.; Speisser, C.; Le Normand, F., HFCVD diamond growth on Cu (111). Evidence for carbon phase transformations by in situ AES and XPS. *Surf. Sci.* **1997,** *387* (1), 28-43.
16. Rümmeli, M.; Grüneis, A.; Löffler, M.; Jost, O.; Schönfelder, R.; Kramberger, C.; Grimm, D.; Gemming, T.; Barreiro, A.; Borowiak-Palen, E., Novel catalysts for low temperature synthesis of single wall carbon nanotubes. *Phys. status solidi (b)* **2006,** *243* (13), 3101-3105.
17. Bae, S.; Kim, H.; Lee, Y.; Xu, X.; Park, J.-S.; Zheng, Y.; Balakrishnan, J.; Lei, T.; Ri Kim, H.; Song, Y. I.; Kim, Y.-J.; Kim, K. S.; Ozyilmaz, B.; Ahn, J.-H.; Hong, B. H.; Iijima, S., Roll-to-roll production of 30-inch graphene films for transparent electrodes. *Nat. Nanotechnol.* **2010,** *5* (8), 574-578.
18. Bolotin, K. I.; Sikes, K. J.; Jiang, Z.; Klima, M.; Fudenberg, G.; Hone, J.; Kim, P.; Stormer, H. L., Ultrahigh electron mobility in suspended graphene. *Solid State Commun.* **2008,** *146* (9–10), 351-355.
19. Lee, C.; Wei, X.; Kysar, J. W.; Hone, J., Measurement of the Elastic Properties and Intrinsic Strength of Monolayer Graphene. *Science* **2008,** *321* (5887), 385-388.
20. Kim, K. S.; Zhao, Y.; Jang, H.; Lee, S. Y.; Kim, J. M.; Kim, K. S.; Ahn, J.-H.; Kim, P.;

Choi, J.-Y.; Hong, B. H., Large-scale pattern growth of graphene films for stretchable transparent electrodes. *Nature* **2009,** *457* (7230), 706-710.

21. Nair, R.; Blake, P.; Grigorenko, A.; Novoselov, K.; Booth, T.; Stauber, T.; Peres, N.; Geim, A., Fine structure constant defines visual transparency of graphene. *Science* **2008,** *320* (5881), 1308-1308.
22. Lee, Y.; Bae, S.; Jang, H.; Jang, S.; Zhu, S.-E.; Sim, S. H.; Song, Y. I.; Hong, B. H.; Ahn, J.-H., Wafer-scale synthesis and transfer of graphene films. *Nano lett.* **2010,** *10* (2), 490-493.
23. Park, J.; Jo, S. B.; Yu, Y. J.; Kim, Y.; Yang, J. W.; Lee, W. H.; Kim, H. H.; Hong, B. H.; Kim, P.; Cho, K., Single-Gate Bandgap Opening of Bilayer Graphene by Dual Molecular Doping. *Adv. Mater.* **2012,** *24* (3), 407-411.
24. Wu, J.; Xie, L.; Li, Y.; Wang, H.; Ouyang, Y.; Guo, J.; Dai, H., Controlled chlorine plasma reaction for noninvasive graphene doping. *J. Am. Chem. Soc.* **2011,** *133* (49), 19668-19671.
25. Guo, B.; Liu, Q.; Chen, E.; Zhu, H.; Fang, L.; Gong, J. R., Controllable N-doping of graphene. *Nano Lett.* **2010,** *10* (12), 4975-4980.
26. Kim, S. J.; Ryu, J.; Son, S.; Yoo, J. M.; Park, J. B.; Won, D.; Lee, E.-K.; Cho, S.-P.; Bae, S.; Cho, S., Simultaneous etching and doping by Cu-stabilizing agent for high-performance graphene-based transparent electrodes. *Chem. Mater.* **2014,** *26* (7), 2332-2336.

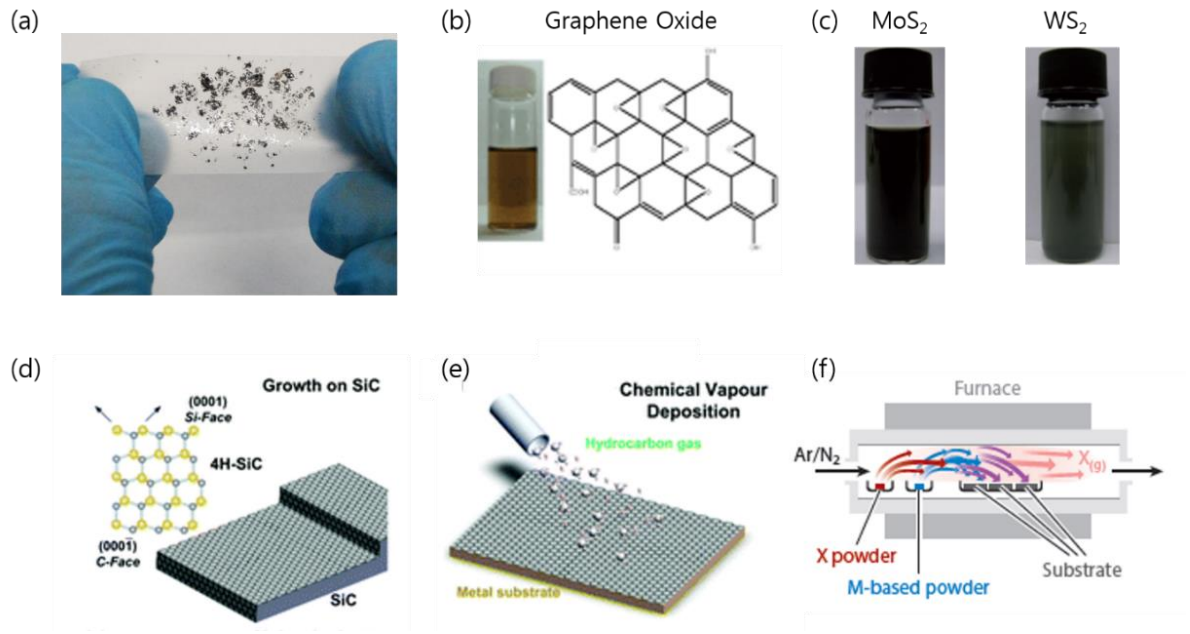

Figure 1. Obtaining the various of methods of layered 2D materials (a) mechanical exfoliation, (b) chemically exfoliated graphene oxide (c) chemically exfoliated MoS_2 and WS_2, (d) epitaxial growth, (e) chemical vapor deposition method of graphene, and (f) of TMDs

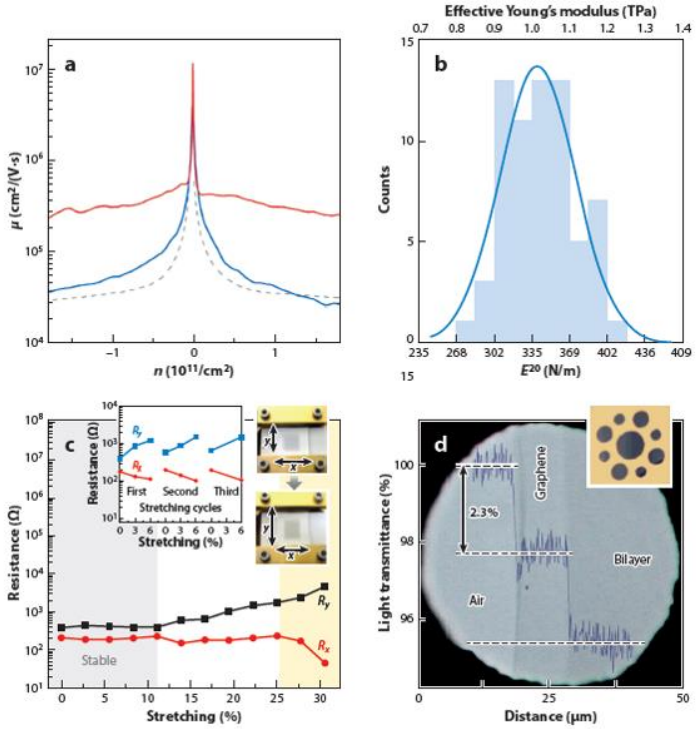

Figure 2. The outstanding properties of graphene for flexible electronics. (a) Mobility as a function of carrier density of a suspended graphene device shows its high electron mobility. (b) Elastic stiffness distribution of graphene film on a silicon oxide cavity. (c) The resistance change of a graphene film transferred onto a polydimethylsiloxane substrate depends on isotropic stretching. (Insets) The resistance change and movement images depend on stretching cycles and stretching direction. (d) Transmittance of partially covered single-layer and bilayer graphene. The inset shows the metal support structure covered with graphene layers.

Chapter 2. Graphene Enhanced Raman Spectroscopy & Photocatalysis

2.1 Introduction

Surface-enhanced Raman scattering (SERS), as a significant optical technique of spectral analysis, is well-known for its ultrasensitive detection, hugely boosting the Raman molecular fingerprint and rapid pre-treatment.[1] The SERS substrate is typically based on a rough surface of a noble metal such as Ag and Au,[2,3] which takes advantage of the huge enhancement of electromagnetic mechanism (EM) compared to other enhancements.

Though there are many controversies about the mechanism, the two types of mechanisms are normally accepted, which are electromagnetic mechanism (EM)[4,5] and chemical mechanism (CM).[6,7] As shown Figure 1, in EM, incident light induces localized surface plasmon resonance. The following enhancement in local field intensity near certain points on the surface brings about substantial increase in Raman cross-section. EM is really a long-range effect that requires the substrate to be rough. While EM attributes the enhancement solely to the substrate, CM is based on interaction between substrate and analyte. CM is usually thought to be a "first layer effect" and a short-range effect, which requires the molecule to be in contact with the substrate or very close to the substrate. In many cases, these two mechanisms coexist, where EM is predominant.

Recently, use of graphene as Raman enhancing substrate has attracted much attention.[8] Comparing with other Raman enhancing technique, such as SERS (surface enhanced Raman spectroscopy) [9-11] or TERS (tip enhanced Raman spectroscopy) [12,13] which use nano-structured novel metals, graphene also has been expected as novel Raman substrate with some unique advantages, depending on its unique electron and phonon structures, atomic uniformity,

biological compatibility, delocalized π bonds and chemical inertness.[8] The process involved is termed graphene-enhanced Raman scattering (GERS) (see the Figure 2a).

Several research groups have successfully demonstrated the clear appearance of Raman signals from graphene-adsorbed dye molecules that are known to hardly show clear Raman spectra because of strong fluorescence backgrounds (Figure 2b).[14,15] This is mainly due to the suppression of molecular fluorescence induced by graphene. However, Ling *et al*. reported that the Raman intensity of various dye molecules all have very different enhancement factor.[16] Moreover, enhancement factors are strongly dependent on probing molecule, on excitation energy of laser, on the material used for the enhancement surface.[17-19] Researcher also reported that the Raman scattering can be enhanced by graphene, similar to the surface enhancement of molecular Raman scattering on metallic surface[9] and studied on the related phenomena in various ways.[20-24]

Recently, it has been reported that not only pristine graphene, but graphene oxide was used in graphene-enhanced Raman spectroscopy. Indeed, oxidized graphene produced by oxidation treatment has dramatically enhanced Raman signal (Figure 2c).[17] Raman enhancement of oxidized graphene results from oxygen group of surface and p-doping effect.

2.1.1 References

1. Guerrini, L.; Graham, D. Molecularly-mediated assemblies of plasmonic nanoparticles for Surface-Enhanced Raman Spectroscopy applications. *Chem, Soc. Rev*. **2012**, 41, 7085-7107.

2. Lin, X. M.; Cui, Y.; Xu, Y. H.; Ren, B.; Tian, Z. Q. Surface-enhanced Raman spectroscopy: substrate-related issues. *Anal. Bioanal. Chem.* **2009**, 394, 1729.

3. Ren, B.; Liu, G. K.; Lian, X. B.; Yang, Z. L.; Tian, Z. Q. Raman spectroscopy on transition metals. *Anal. Bioanal. Chem.* **2007**, 388, 29.

4. Schatz, G. C.; Young, M. A.; Van Duyne, R. P. Electromagnetic mechanism of SERS. *Top. Appl. Phys*. **2006**, 103, 19–46.

5. Schatz, G. C.; Duyne, R. P. V. D. Electromagnetic Mechanism of Surface-enhanced Spectroscopy. *Surface-enhanced Vib. Spectrosc*. **2002**, 1–16.

6. Campion, A.; Ivanecky, J. E.; Child, C. M.; Foster, M. On the Mechanism of Chemical Enhancement in Surface-Enhanced Raman Scattering. *J. Am. Chem. Soc*. **1995**, 117 (47), 11807–11808.

7. Fromm, D. P.; Sundaramurthy, A.; Kinkhabwala, A.; Schuck, P. J.; Kino, G. S.; Moerner, W. E. Exploring the chemical enhancement for surface-enhanced Raman scattering with Au bowtie nanoantennas. *J. Chem. Phys*. **2006**, 124 (6), 1–9.

8. Xu, W.; Mao, N.; Zhang, J. Graphene: a platform for surface-enhanced Raman spectroscopy. *Small* **2013**, 9 (8), 1206–1224.

9. Nie, S.; Emory, S. R. Probing Single Molecules and Single Nanoparticles by Surface-Enhanced Raman Scattering. *Science* **1997**, 275 (5303), 1102–1106.

10. Kneipp, K.; Wang, Y.; Kneipp, H.; Perelman, L. T.; Itzkan, I.; Dasari, R. R.; Feld, M. S. Single Molecule Detection Using Surface-Enhanced Raman Scattering (SERS). *Phys.*

Rev. Lett. **1997**, 78 (9), 1667–1670.

11. Lee, P. C.; Meisel, D. Adsorption and surface-enhanced Raman of dyes on silver and gold sols. *J.Phys.Chem*. **1982**, 86 (17), 3391–3395.
12. Stöckle, R. M.; Suh, Y. D.; Deckert, V.; Zenobi, R. Nanoscale chemical analysis by tip-enhanced Raman spectroscopy. *Chem. Phys. Lett.* **2000**, 318 (1-3), 131–136.
13. Pettinger, B.; Ren, B.; Picardi, G.; Schuster, R.; Ertl, G. Nanoscale Probing of Adsorbed Species by Tip-Enhanced Raman Spectroscopy. *Phys. Rev. Lett.* **2004**, 92 (9), 096101–1.
14. Xie, L.; Ling, X.; Fang, Y.; Zhang, J.; Liu, Z. Graphene as a substrate to suppress fluorescence in resonance Raman spectroscopy. *J. Am. Chem. Soc*. **2009**, 131 (29), 9890–9891.
15. Ling, X.; Xie, L.; Fang, Y.; Xu, H.; Zhang, H.; Kong, J.; Dresselhaus, M. S.; Zhang, J.; Liu, Z. *Nano Lett*. **2010**, 10 (2), 553–561.
16. Ling, X.; Xie, L.; Fang, Y.; Xu, H.; Zhang, H.; Kong, J.; Dresselhaus, M. S.; Zhang, J.; Liu, J. Can graphene be used as a substrate for Raman enhancement? *Nano Lett.* **2010**, 10, 553.
17. Huh, S.; Park, J.; Kim, Y. S.; Kim, K. S.; Hong, B. H.; Nam, J.-M. UV/ozone-oxidized large-scale graphene platform with large chemical enhancement in surface-enhanced Raman scattering. *ACS Nano* **2011**, 5, 9799.
18. Yu, X.; Cai, H.; Zhang, W.; Li, X.; Pan, N.; Luo, Y.; Wang, X.; Hou, J. G. Tuning chemical enhancement of SERS by controlling the chemical reduction of graphene oxide nanosheets. *ACS Nano* **2011**, 5, 952-958.
19. Liu, C.-Y.; Liang, K.-C.; Chen, W.; Tu, C. hao; Liu, C.-P.; Tzeng, Y. Plasmonic coupling of silver nanoparticles covered by hydrogen-terminated graphene for surface-enhanced Raman spectroscopy. *Opt. Express* **2011,** 19, 17092-17098.

20. Ling, X.; Zhang, J. Interference Phenomenon in Graphene-Enhanced Raman Scattering. *J. Phys. Chem. C* **2011**, 115 (6), 2835–2840.

21. Xu, H.; Chen, Y.; Xu, W.; Zhang, H.; Kong, J.; Dresselhaus, M. S.; Zhang, J. Modulating the charge-transfer enhancement in GERS using an electrical field under vacuum and an n/p-doping atmosphere. *Small* **2011**, 7 (20), 2945–2952.

22. Ling, X.; Moura, L. G.; Pimenta, M. A.; Zhang, J. Charge-Transfer Mechanism in Graphene-Enhanced Raman Scattering. *J. Phys. Chem. C* **2012**, 116 (47), 25112–25118.

23. Ling, X.; Wu, J.; Xu, W.; Zhang, J. Probing the Effect of molecular orientation on the intensity of chemical enhancement using graphene-enhanced Raman spectroscopy. *Small* **2012**, 8 (9), 1365–1372.

24. Yaghobian, F.; Korn, T.; Schüller, C. Frequency Shift in Graphene-Enhanced Raman Signal of Molecules. *Chem. Phys. Chem.* **2012**, 13 (18), 4271–4275.

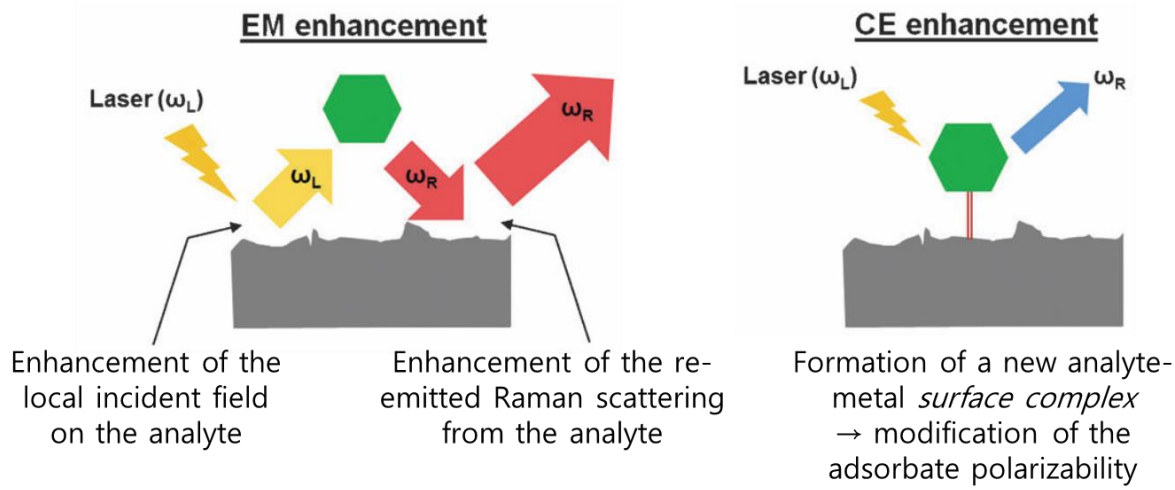

Figure 1. Schematic of the electromagnetic and chemical enhancements in SERS.[1]

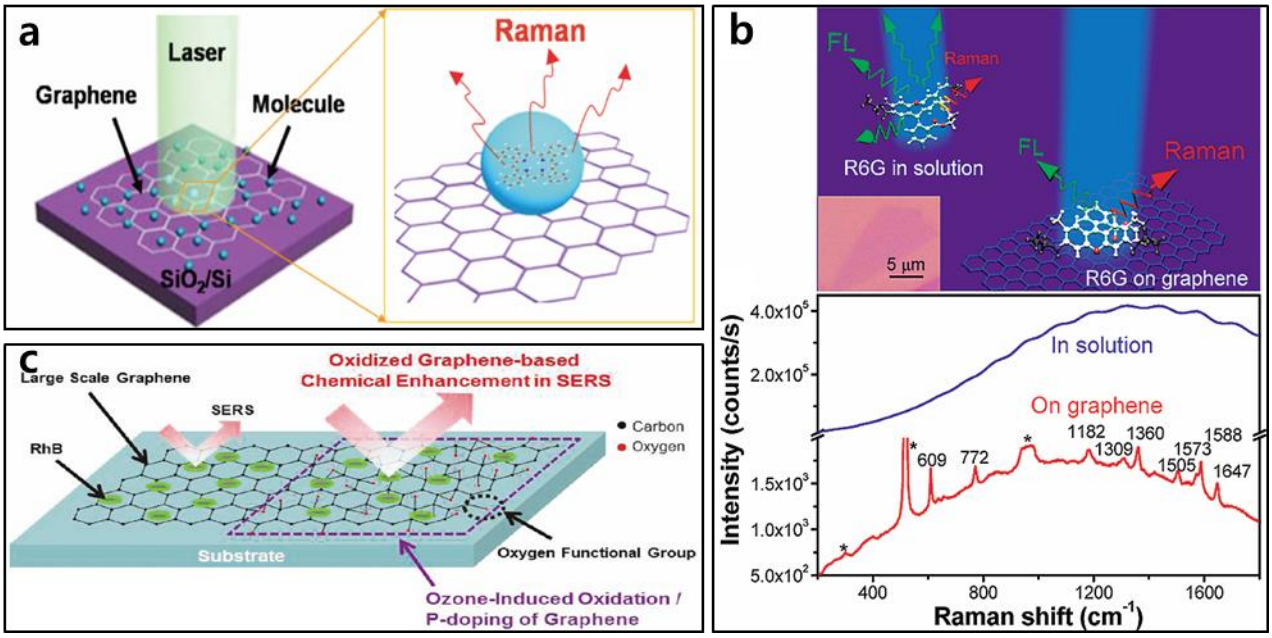

Figure 2. (a) Schematic illustration of the molecules on graphene and a SiO_2/Si substrate, and the Raman experiments.[16] (b) Schematic illustration and Raman spectra of R6G in water (10 μM) (blue line) and on a graphene film (red line) at 514 nm excitation.[14] (c) Schematic diagram of the UV/ozone oxidized graphene-based chemical enhancement in SERS.[17]

2.2 Graphene-Sandwiched Resonance Raman Spectroscopy

2.2.1 Introduction

The mechanism of graphene-enhanced Raman spectroscopy (GERS) has not been clearly established, chemical mechanism (CM) rather than electromagnetic mechanism (EM) has been generally adopted to explain such GERS, due to the relatively flat surface of graphene.[1] However, more recently, it has been reported that the actual Raman scattering cross-sections of dye molecules (R6G) decrease on graphene surface, evidenced by micro-optical contrast spectroscopy and Raman scattering measurements, and GERS is qualitatively explainable by a model incorporating the EM rather than by a model of CM.[1] The origin of GERS has been controversial since its discovery. [2,3]

Under these backgrounds, we first examined resonance Raman spectra of some representative dye molecules in order to understand the enhancement mechanism of GERS. Structural confinement is newly introduced as a novel parameter, by making sandwich structures as covering target molecules with another graphene layer. The result is well explainable by the conventional mechanism of resonance Raman spectroscopy, especially for planar dye molecules.

Secondly, for nonplanar dye molecules, we could observe the abnormal Raman enhancement regardless of their molecular resonance overlap with excitation laser when sandwiched between graphene layers. We proposed the existence of another resonance condition for this abnormal enhancement, which is quantum void resonance. Through the examination of a few supposed hypotheses, it could be adopted that the molecular sized void structure, which is generated by tilted configuration of nonplanar dye when confined between

graphene layers, is regarded as to play the role in abnormal Raman enhancement.

2.2.2 Experimental

Graphene Synthesis Graphene was synthesized on a copper foil by CVD (chemical vapour deposition) method. As-synthesized graphene was coated by poly(methyl methacrylate) (PMMA) and copper foil was removed using by typical etchant of ammonium persulfate solution, then the graphene was transferred on SiO_2 (300nm) / Si substrate after rinsed with copious distilled water. After the removal of PMMA by soaking in acetone, the graphene was annealed at 320℃ under inert hydrogen and helium gas atmosphere.

Sample Preparation. Acridine orange (99%), nile red (98%), methylene blue (95%), rhodamine 123 (95%), rhodamine 6G (95%), rhodamine B (95%), coomassie brilliant blue g250 and xylene cyanol ff were purchased from Sigma Aldrich and used without further purification. The graphene sample was dipped in 200 μM aqueous or ethanolic dye solution for an hour and rinsed with water or ethanol and dried before Raman measurements.

Regarding concentration issue for adsorbed dye, we were referenced by the examination in the previous work.[4] They revealed that contrast spectroscopy provides how the dye adsorbed on graphene surface and with using the refractive index value it was revealed that the dye coverage adsorbed from 1 mM solution is approximately 1-2 monolayers. In our experiments, five times diluted solution of 200 μM should provide the coverage below 1-2 monolayers of dye.

To fabricate dye encapsulated sandwich structure sample was covered by PMMA-supported single layered graphene floated on water and PMMA was removed by acetone (not heated) before optical measurements.

To exclude the effect of encapsulated water on Raman enhancement our recently developed graphene transfer method (dry method via Self Adhesive Film (SAF) for ultra-clean

transfer) was used for fabricating the sandwich sample[5] and revealed that similar Raman enhancement of dye was successfully observed.

Characterization. For UV-vis absorption measurements (SCINCO S-4100), as-prepared dye on graphene or sandwiched samples are laid on 0.5 mm thickness quartz substrate. All spectrums in the manuscript were calibrated by subtracting the spectrum of bare single layered (or two layered for sandwich sample) graphene sheets on quartz from original one.

Raman measurements were conducted using Invia Renishaw Raman spectrometer (RM 1000) with 514.5 nm and 633 nm laser line. (~0.5 mW).

The theoretical calculation of Raman spectra of R6G was performed with density functional theory (B3LYP-6-31G (d,p)) using the GAUSSIAN software.

2.2.3 Results and Discussion

Figure 3 represents red-shift of molecular absorbance induced by graphene layers. Due to the high local polarizability of graphene, it is known that absorption spectra of molecules (solid line) shifted about 10 nm to longer wavelength (dashed line) when adsorbed on graphene.[4,6] Whereas, when the molecules sandwiched between two graphene layers, the second graphene layer is expected to bring about further red-shift (dotted line) of molecular resonance by covering the molecule. Therefore, the resonance with laser excitation would increase or decrease as graphene layers are added, depending on whether the shifted absorbance matches more or less with the laser excitation wavelength. The Raman cross-section is expected to increase when the resonance gets larger, and decrease in opposite cases.

We categorized the dye molecules into two groups depending upon their geometric planarity. Acridine orange (AO), nile red (NR), and methylene blue (MB), which have extinction maxima at 492, 548, 656 nm, respectively, belong to planar dyes because they all have fully conjugated pi electron structure as is shown in Figure 4a. Figure 4b shows absorbance spectra of them. AO and NR have maxima near 514.5 nm, thus they show clear resonance Raman spectra at 514.5 nm laser, while not at 633 nm. On the other hand, MB shows clear Raman feature only at 633 nm. We observed the change in resonance Raman spectra of those planar dye molecules when sandwiched between two graphene layers, compared with ordinary GERS condition that target molecules are adsorbed on a single graphene layer. In the case of AO, since its maximum peak occurs at shorter wavelength than laser excitation, it is expected to become resonant more with the laser as its spectrum is red-shifted. Therefore, the resonance Raman scattering intensity of AO sandwiched between graphene is larger than AO on a single layer (Figure 5). In contrast, in the cases of NR and MB, their maxima peaks are located at longer wavelength than their respective laser excitation. Accordingly, the red-shifts

induce less resonance with laser, causing decrease in resonance Raman scattering intensity when sandwiched between graphene layers (Figure 4d and Figure 5). These results with planar molecules are in accordance with our expectation, that the extent of molecular resonance with excitation wavelength has close relationship with Raman scattering cross-section. Figure 4c shows experimental UV-vis absorbance spectra of methylene blue (MB) adsorbed on graphene surface (black line) and sandwiched between two graphene sheets (red line), which present apparent spectral red shift along with slight decrease of absorbance corresponding to the changes in electronic resonance of dye. The overlap between molecular absorbance and excitation laser (633 nm) decreases according to the spectral red shift. This is already mentioned several years ago in the paper written by L. Brus *et al.*[6]

Unlike planar dye, nonplanar dye assumes unexpected aspects. Figure 6a and b represents molecular structure and absorbance spectra of Rhodamine 123 (Rh-123), Rhodamine 6G (R6G), Rhodamine B (Rh-B), Coomassie Blue g250 (CB-g250), and Xylene Cyanol ff (XC-ff), which have extinction maxima at 501, 527, 554, 584, 616 nm, respectively. Rh-123, R6G, and Rh-B show resonance Raman spectra at 514.5 nm, while CB-g250 and XC-ff at 633nm. According to the previous explanation of planar molecules, the Raman scattering intensity depends on the extent of molecular resonance with laser excitation. Rh-123, CB-g250, and XC-ff have maxima peaks at shorter wavelength than laser excitation. Thus, red-shifts induced from graphene sandwich structure make them more resonant and increases in resonance Raman scattering intensity are anticipated compared with normal GERS (Figure 7). On the contrary, R6G and Rh-B have extinction maxima at lower energy than laser excitation. Hence, resonance Raman scattering intensity of sandwich structure is expected to be lower than that of unconfined structure. However, surprisingly, all of them show significant increase in Raman intensity (Figure 6d and Figure 7).

To understand the abnormal increase in Raman intensity of R6G and Rh-B, we, at first, carefully examine how the electronic resonance changes according to the structure. Figure 6c shows UV-vis absorbance of R6G dye adsorbed on single graphene surface and the one sandwiched between two graphene sheets. Absorbance increase was clearly detected and induced more overlap with 514. 5 nm excitation laser line, which in turn generate enhanced resonant Raman intensity. Considering both that the graphene itself has no significant absorbance in the visible region and that the planar dye showed spectral shift (also with slight decrease of absorbance for methylene blue) in Figure 4c, the absorbance increase without spectral shift here might have strong relationship with molecular geometry of nonplanar dye.

On the other hand, Figure 8a shows that nonplanar dye molecule such as R6G consists of xanthene ring and phenyl ring moiety in its structure. Because of steric hindrance between them, phenyl ring must be out of plane with respect to xanthene ring plane. Thus, when adsorbed on graphene, it inevitably situated as tilted configuration, which means partial pi-pi stacking between xanthene ring and graphene surface, while planar dye such as acridine orange, nile red, and methylene blue, they all only have fully pi-conjugated ring structure (Figure 4a) without any bulky group such as phenyl ring, thus more efficiently adsorbed on graphene surface via pi-pi interaction. Considering that xanthene is the main fluorophore in R6G molecule, partial pi-pi interaction of xanthene with graphene inevitably induces weak fluorescence quenching efficiency by graphene when irradiated by excitation laser.

This is spectroscopically verified by comparing fluorescence background intensity observed in Raman spectra. Figure 8b shows that the background signal measured at GERS substrate of all nonplanar dye is significantly intense than the one of all planar dyes. Close proximity of planar dye with graphene induces strong quenching of fluorescence, thus exhibits relatively weak fluorescence background, while the tilted configuration of nonplanar dye

induces partial quenching of fluorescence, thus generates rather stronger fluorescence background. This is schematically drawn in Figure 9.

When nonplanar R6G dye, which has already tilted configuration on graphene (GERS substrate), was covered by second graphene layer upon the molecule, it is expected that molecular sized void structure is made because of volumetric property of nonplanar dye and also with high mechanical flexibility of graphene, which is schematically drawn in Figure 8a (sandwich structure). In this structure, it is believed that very small sized void space (quantum void) should be generated between upper and lower graphene.

Here, we suggest that the observed abnormal increase of Raman signal in sandwich structure of R6G and Rh-B in Figure 6e is originated from this quantum void structure. Enhanced molecular absorbance (Figure 6c) along with strong fluorescence background (Figure 8b) is the strong evidence of existence of newly generated excited state of nonplanar dye in sandwich structure. In the basic principle of resonance Raman spectroscopy, Raman scattering is occurred involving the transition between ground state with an excited real electronic state, not a virtual state. In this regard, enhanced absorbance (fluorescence background) strongly supports the existence of real excited state not a virtual state.

In addition, interestingly, Raman peaks of graphene also increased at nonplanar dye intercalated sandwich graphene structure. This is another evidence of quantum void induced-resonance, which provides resonance condition for intercalated dye species along with surrounding graphene.[7] Summarized data is shown in Figure 10.

On the other hand, one might think that Raman signal of R6G sandwiched between graphene can be enhanced by the effect of more conjugation of pi electron of phenyl ring with xanthene ring induced by flattening of molecular structure via pressed graphene. To examine this assumption, we conducted the DFT calculation of R6G and obtained the Raman spectra as

the changes of dihedral angle between phenyl ring and xanthene ring plane. As shown Figure 11, Raman intensity has not been changed significantly until 40 degree. Rather, new vibrational bands start to appear from the angle of 50 degree, which was not observed in our experimental data in Figure 6d. Also, the relative ratio (not an absolute value) of peak position, intensity and band width among the peaks in sandwich structure are not changed compared to the ones in GERS substrate. These results rule out the possibility of rotation of phenyl ring.

In application, not only signal enhancement is the useful advantageous point used as Raman spectroscopic analyzing substrate, but also chemical robustness is another merit of sandwich structure compared with one in GERS. Previous GERS substrate cannot preserve the adsorbed dye, while our sandwich structure perfectly protects the inner dyes from dissolving out by strong organic solvent like acetone as a function of barrier.

2.2.4 Conclusion

There has been no report about the GERS effect for non-resonant molecules without any supporting material such as noble metal nanoparticles. From its first discovery, all observations using GERS effect have been limited on the dye molecules, which should be detected by resonant excitation wavelength. However, by investigating the Raman response of graphene-dye sandwich structure according to the geometric planarity of encapsulated dye, we first reached the successful elucidation of the function of graphene in GERS with planar dye. Secondly, we observed the molecular resonance-irrespective abnormal enhancement of Raman signal from nonplanar dye, which is originated from the molecular geometric effect when confined between graphene as sandwiched structure. Considering that much of organic dyes in chemical library have nonplanar molecular structure, our sandwich structure can be easily used as novel Raman analyzing platform for detection of dyes also with chemical robustness of the structure.

2.2.5 References

1. Ling, X.; Zhang, J. First-layer effect in graphene-enhanced Raman scattering. *Small* **2010**, 6 (18), 2020–2025.

2. Deng, S.; Xu, W.; Wang, J.; Ling, X.; Wu, J.; Xie, L.; Kong, J.; Dresselhaus, M. S.; Zhang, J. Direct measurement of the Raman enhancement factor of rhodamine 6G on graphene under resonant excitation. *Nano Res.* **2014**, 7 (9), 1271–1279.

3. Huang, S.; Ling, X.; Liang, L.; Song, Y.; Fang, W.; Zhang, J.; Kong, J.; Meunier, V.; Dresselhaus, M. S. Molecular selectivity of graphene-enhanced Raman scattering. *Nano Lett.* **2015**, 15 (5), 2892-2901.

4. Thrall, E. S.; Crowther, A. C.; Yu, Z.; Brus, L. E. R6G on graphene: high Raman detection sensitivity, yet decreased Raman cross-section. *Nano Lett.* **2012**, 12 (3), 1571–1577.

5. Kim, S. J.; Choi, T.; Lee, B.; Lee, S.; Choi, K.; Park, J. B.; Yoo, J. M.; Choi, Y. S.; Ryu, J.; Kim, P.; Hone, J.; Hong, B. H. Ultraclean patterned transfer of single-layer graphene by recyclable pressure sensitive adhesive films. *Nano Lett*. **2015**, 15 (5), 3236–3240.

6. Jung, N.; Crowther, A. C.; Kim, N.; Kim, P.; Brus, L. Raman Enhancement on Graphene: Adsorbed and Intercalated Molecular Species. *ACS Nano* **2010**, 4 (11), 7005–7013.

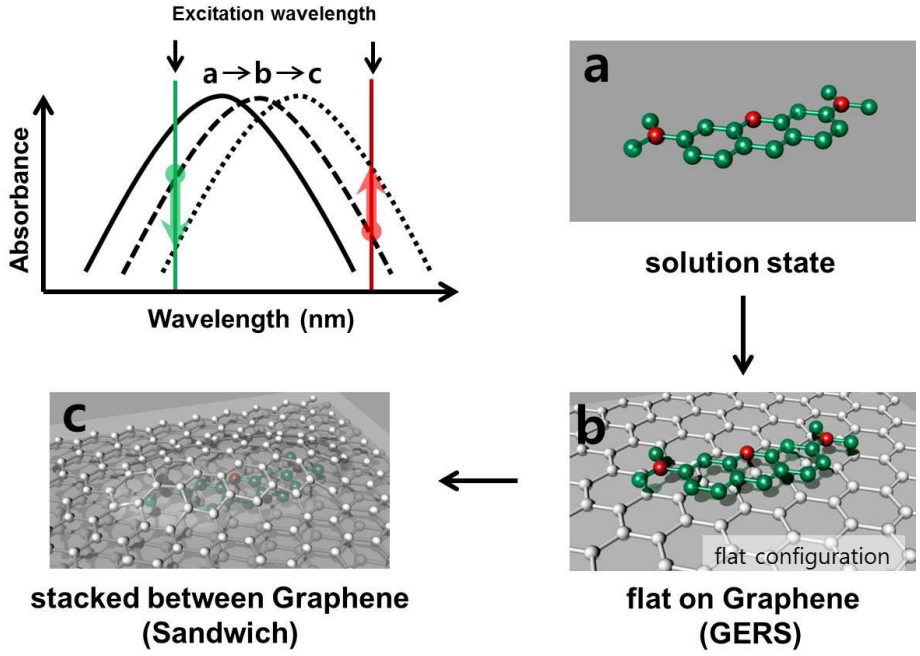

Figure 3. Schematic presentation for resonance change of planar dye. (a) Planar acridine orange of solution state. (b) Adsorbed state of acridine orange on graphene surface with flat configuration. (c) Sandwiched state of acridine orange between two single layered graphene with flat configuration.

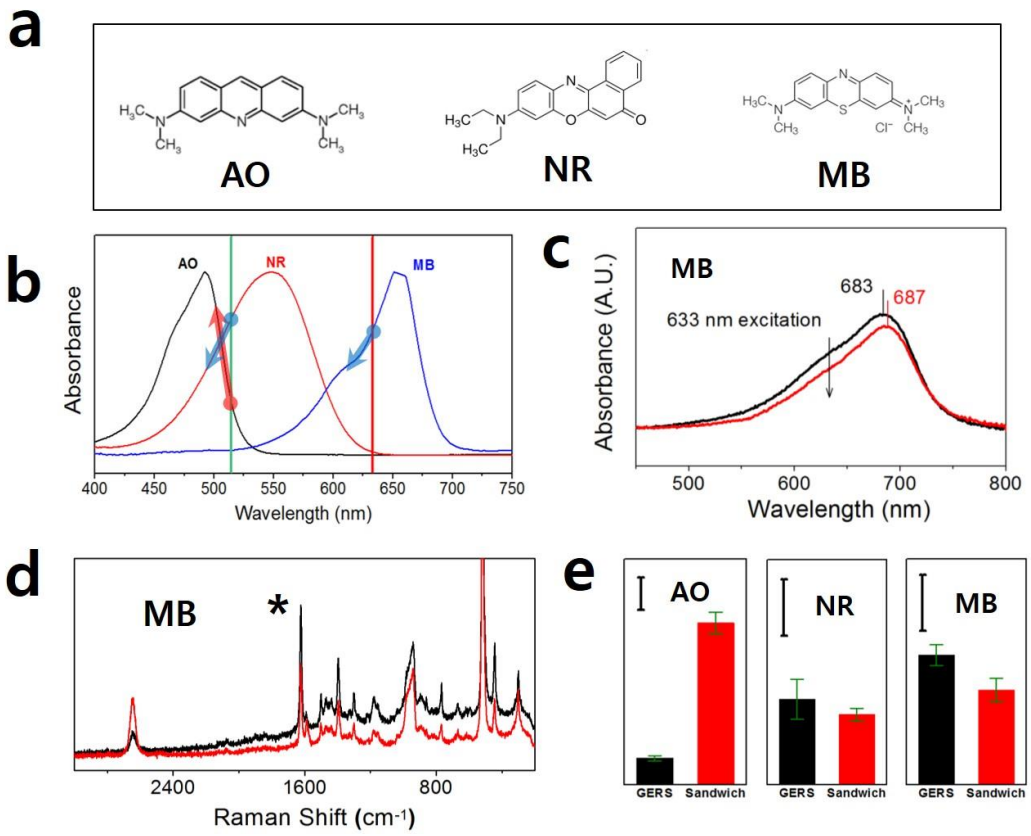

Figure 4. (a) Molecular structure of planar dyes used in the experiments (b) Absorbance of bulk sample of three planar dyes of acridine orange (AO), nile red (NR), and methylene blue (MB) dispersed in ethanol. Two vertical lines are excitation laser wavelengths of 514.5 and 633 nm used for resonance Raman measurements. (c) Absorbance spectra of methylene blue at adsorbed state on graphene surface (black line) and sandwiched state between graphene (red line) (d) Raman spectra of MB dye measured at 633 nm for adsorbed state on graphene surface (black, GERS substrate) and sandwiched state between graphene (red, our sandwich substrate). See the supporting information for the Raman spectra of AO and NR. (e) Baseline-subtracted Raman intensity of the peak denoted as asterisk in spectra of (d). G and 2D peak of graphene are clearly shown at ~1590 and ~2645 cm^{-1}, respectively. Scale bar stands for 1000 Raman counts in our experimental condition.

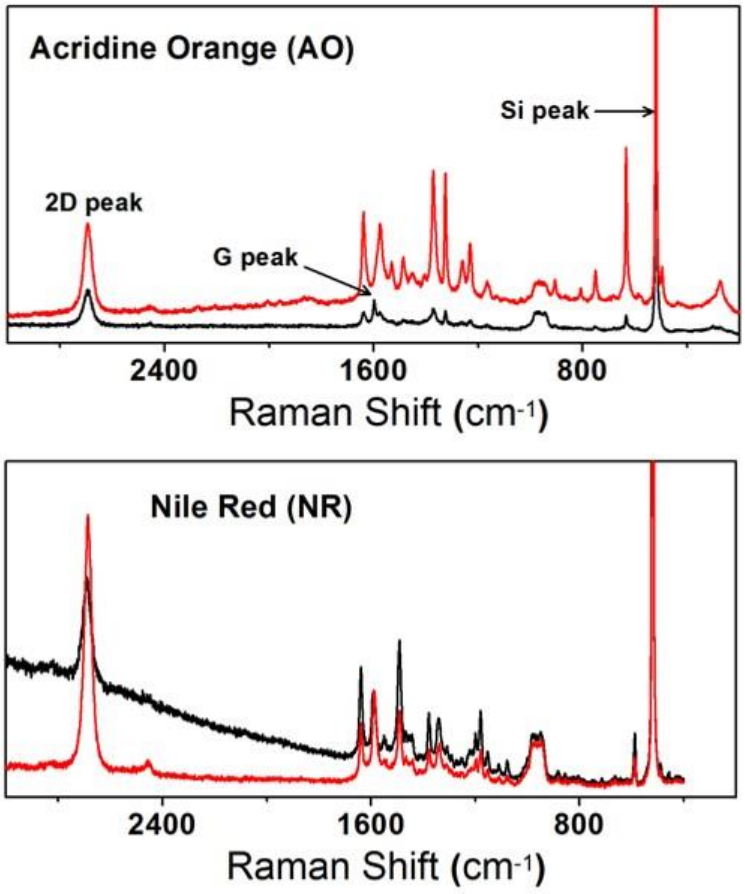

Figure 5. Raman spectra of planar dye of Acridine Orange (AO) and Nile Red (NR) adsorbed on graphene surface (black) and sandwiched between two graphene sheets (red).

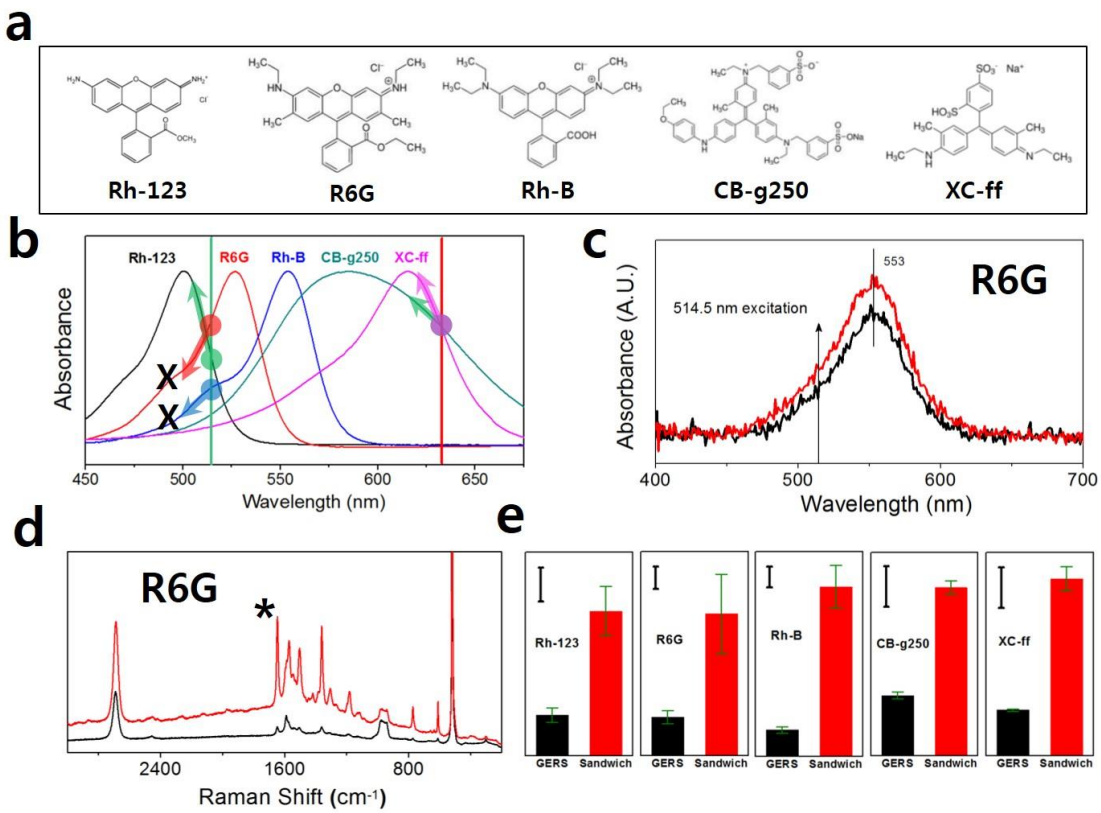

Figure 6. (a) Molecular structure of nonplanar dyes used in the experiments (b) Absorbance of five nonplanar dyes of rhodamine 123 (Rh-123), rhodamine 6G (R6G), rhodamine B (Rh-B), coomassie brilliant blue g250 (CB-g250), and xylene cyanol ff (XC-ff) dispersed in ethanol. Two vertical lines are excitation laser wavelengths of 514.5 and 633 nm used for resonance Raman measurements. (c) Absorbance spectra of R6G at adsorbed state on graphene surface (black line) and sandwiched state between graphene (red line) (d) Raman spectra of nonplanar dye measured at 514.5 nm from adsorbed state on graphene surface (black, GERS substrate) and sandwiched state between graphene (red, our sandwich substrate). (c) Baseline-subtracted Raman intensity of the dye peak denoted as asterisk in spectra of (b). G and 2D peak of graphene are clearly shown at ~1589 and ~2690 cm^{-1}, respectively. Scale bar stands for 1000 Raman counts.

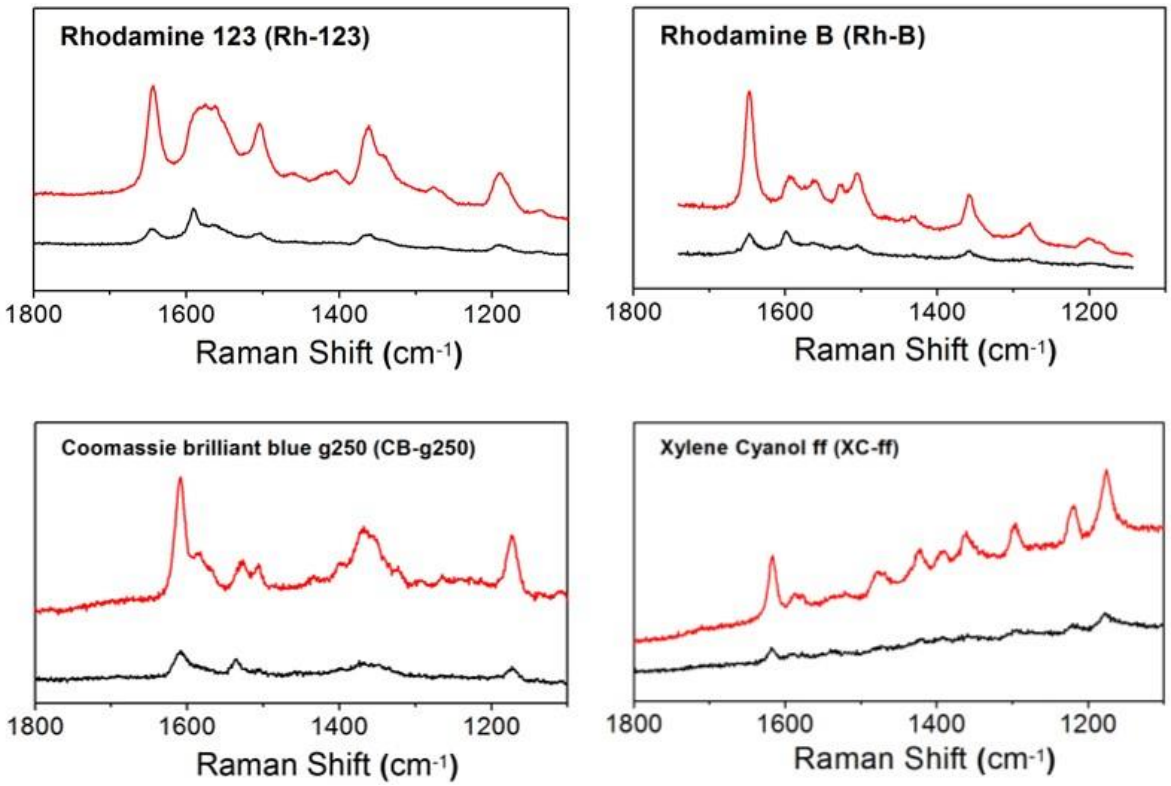

Figure 7. Raman spectra of nonplanar dye of rhodamine 123 (Rh-123), rhodamine B (Rh-B), coomassie brilliant blue g250 (CB-g250), and xylene cyanol ff (XC-ff) adsorbed on graphene surface(black) and sandwiched between two graphene sheets (red).

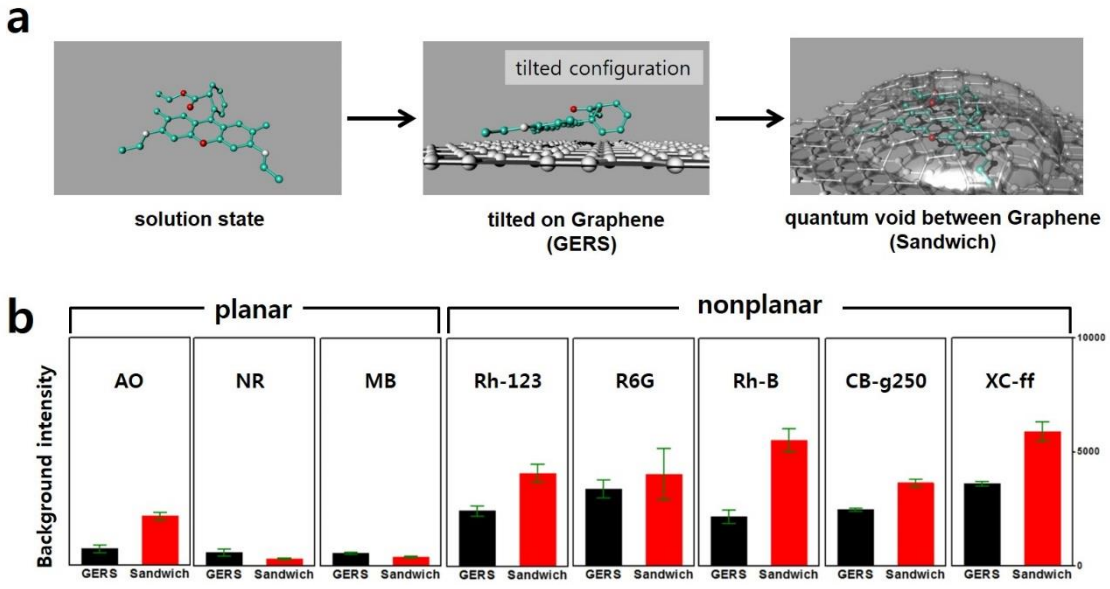

Figure 8. Schematic representation of mechanism of Raman signal enhancement of nonplanar dye observed in Figure 6. (a) Encapsulation of nonplanar dye (R6G) between graphene. (b) Comparison of background intensity of planar dye and nonplanar dye extracted from the Raman spectra in Figure 4 and Figure 6 (baseline Raman scattering intensity at the position of peak denoted as asterisk).

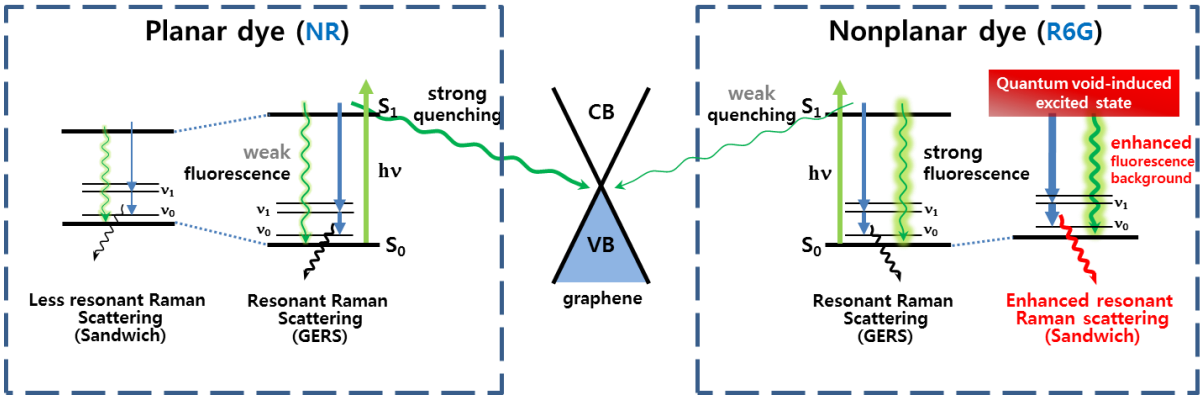

Figure 9. Scheme for comparing the fluorescence quenching efficiency and Raman scattering intensity between the case of planar dye and nonplanar dye.

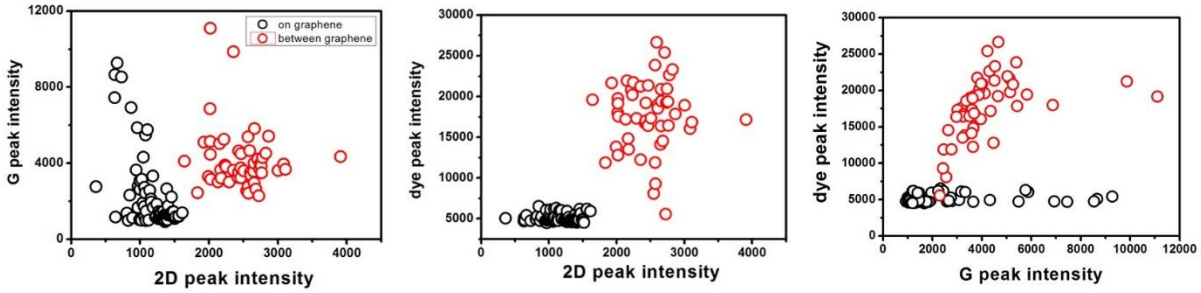

Figure 10. Raman intensity variation of nonplanar dye (XC-ff, xylene cyanol-ff), graphene G and graphene 2D peaks according to the structure. It shows that all Raman signals (dye, G, 2D) in 'dye-**between**-two sheets of graphene' structure are enhanced compared to the 'dye-**on**-two sheets of graphene' structure.

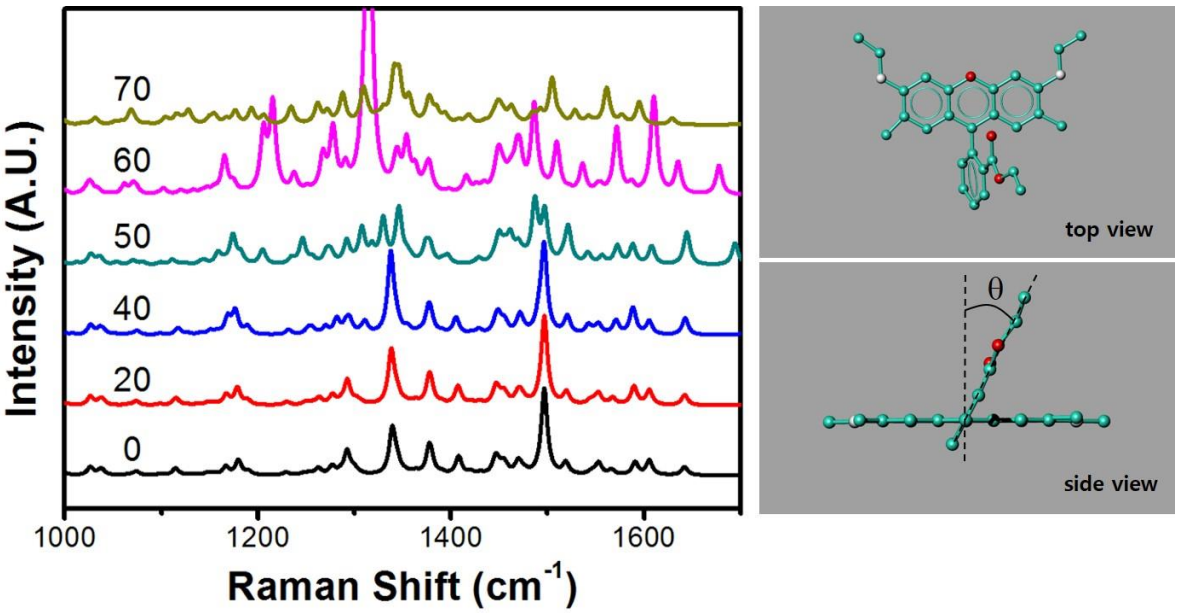

Figure 11. DFT calculation (B3LYP 6-31G(d,p) level, GAUSSIAN 03W) results of Raman spectra of rhodamine 6G according to the change of dihedral angel between xanthene and phenyl ring planes. As the dihedral angle increases, Raman intensity has not been changed significantly until 40 degree. Rather, new vibrational bands start to appear from the angle of 50 degree, which was not observed in our experimental data in Figure 6d.

2.3. Graphene-Catalyzed Photoreduction of Dye Molecules

2.3.1 Introduction

Although graphene is composed of only carbon atoms,[1,2] its electrical properties are similar to that of novel metals that can provide or stabilize charge carriers for chemical reactions. Thus, graphene is expected to show excellent electrochemical or photochemical catalytic properties that are useful for various energy and environmental applications.[3] However, for these catalytic applications of graphene, a combination with photosensitizing materials is essential to generate photo-excited charge carriers because graphene shows negligible absorption in the visible range. Therefore, to the best of our knowledge, there has been no report on the photocatalytic activity of graphene without any photosensitizing additives.

Herein, we report, for the first time, that the single layer graphene can catalyze the photoreduction of nitrobenzene dye compounds, revealed by graphene-enhanced Raman spectroscopy (GERS).[4] Since the observation of Raman signal enhancement for the molecules on graphene, graphene has also attracted much attention of researchers as a part of surface-enhanced Raman scattering (SERS). It has been reported that not only the enhancing phenomena of Raman signals, but also the enhancement mechanism of GERS. Unlike on the metal, ground-state charge transfer can easily occur between graphene and the molecule, because graphene has considerable p electrons and its energy band is continuous.[5] Moreover, the GERS effect strongly depends on the precise electronic structure of the molecule and also on the energy gap between the HOMO and LUMO states of the molecule.[6]

Disperse Red 1 (DR1) known as a famous push–pull azobenzene derivative molecule was employed to study the graphene-catalyzed photoreduction reaction.[7] DR1 has been intensively

studied due to its unique photo-switchable trans–cis isomerization reaction,[8,9] which is found to be quenched due to the strong π–π interaction between DR1 and graphene. In addition, the ultrafast hole transfer from photo-excited DR1 to graphene also disables the recombination of electron–hole pairs. DR1 covered or sandwiched with graphene shows less photocatalytic reaction, implying that ambient air provided the hydrogen sources essential for the photoreduction of nitrobenzene into aniline functionalities.

The overall experimental results indicate that the electron is transferred from the valence band of graphene to the photo-excited empty HOMO as shown in Figure 12a. Consequently, the photoluminescence of DR1 is suppressed because the temporary hole state is filled by the electron from graphene (process 2 in Figure 12a), which makes Raman spectra visible by quenching fluorescence background. In stoichiometry, the overall reaction requires 6 electrons and 3 hydrogen molecules (H_2), leaving 2 water molecules (H_2O) as byproducts. The reduced DR1 reacts with the first H_2 to convert $–NO_2$ to –NO, the second H_2 forms –NHOH, and the final H_2 completes the reaction into $–NH_2$ (Figure 12b).[10]

2.3.2 Experimental

Sample Preparation. Graphene was synthesized on a copper foil by CVD (chemical vapour deposition) method. As-synthesized graphene was coated by poly(methyl methacrylate) (PMMA) and copper foil was removed using by typical etchant of ammonium persulfate solution, then the graphene was coated on SiO_2 (300nm) / Si substrate after rinsed with copious distilled water. After the removal of PMMA, the graphene was annealed at 320℃ under inert hydrogen and helium gas atmosphere. The sample was dipped in 200μM ethanolic solution of DR1 for an hour before Raman measurements.

Deposition Molecules on UV/Ozone-oxidized graphene. To oxidize surface of graphene, graphene on SiO_2/Si substrate was exposed to UV light source for 5 or 10 minute using UV/ozone cleaner (Bioforce). The sample was immersed in 200μM DR 1 aqueous solution for an hour and washed with deionized water.

Characterization. All Raman measurements were conducted using Invia Renishaw Raman spectrometer (RM 1000) with 514.5 nm laser line. (~0.5 mW). The theoretical calculation of Raman spectra were performed with density functional theory (B3LYP-6-31G (d,p)).

2.3.3 Results and Discussion

Raman spectroscopy was employed to elucidate the mechanism of the graphene-catalyzed photoreduction reaction. Usually, dye molecules have strong photoluminescence (PL) that overwhelms the Raman signal, but the graphene-assisted PL quenching is extremely helpful to investigate their vibrational features related to molecular structures and functionalities. In field of Raman spectroscopy, graphene has been mainly studied GERS effect, however, we suggested that catalytic effect of graphene at the photoreduction as well as enhancement effect. We actually observed the enhancement of DR1 based on GERS (Figure 13).

Figure 14a shows the Raman spectra of DR1 molecules adsorbed on a single-layer graphene on a SiO_2 (300 nm)/Si substrate. Graphene was synthesized by a typical chemical vapor deposition (CVD) method and transferred by spin-coated PMMA. After the removal of PMMA, graphene is annealed at 320℃ to remove polymer residues.

The Raman spectra exhibit the clear features of DR1. The peaks at 1102, 1134, 1194, 1334, 1387, 1422, 1444 and 1588 cm^{-1} can be assigned to the δ(C–H), ν(C–N), δ(C–H), ν(N–O), ν(N=N), ν(C–C), ν(C–C) and ν(C–C), respectively. While monitoring the spectrum during irradiation using a 514.5 nm laser, we observed apparent changes in some vibrational bands. The peak at 1334 cm^{-1} corresponding to ν(N–O) decreased gradually, while the peak at 1120 cm^{-1} and 1134 cm^{-1} corresponding to the amine groups increased.

In this study, it is experimentally difficult to control the final product mixture between nitro-DR1 and amino-DR1. Instead, to confirm the peak resulted from reduction, we observed the Raman spectra of 4’-amino-4’-dimethylamine azobenzene (4’-amino-DAB), which is structurally similar to amino-DR1. Although this molecule is composed of dimethyl group instead of ethyl and ethanol group in DR1, these differences might be negligible in this wavenumber range. To exclude catalyzed effect of graphene, all spectra were measured as

normal Raman spectrum using powder samples without graphene. In Figure 15, the peaks at 1334 cm^{-1} corresponding to ν(N-O) of DR1 decreased gradually after irradiation of 514.5nm laser, on the other hand, the peak at 1120 cm^{-1} corresponding amine group increased. It is consistent with results obtained the spectrum of 4'-amino-DAB.

To clearly confirm the origin of peak change, the DFT calculation of the Raman spectrum was conducted for DR1. Figure 14b shows the mixed Raman spectrum of nitro-DR1 and amine-DR1 at each ratio. As more amine-DR1 is generated from nitro-DR1, the peak at 1338 cm^{-1} decreases noticeably while peaks at 1118 and 1130 cm^{-1} increase with respect to the one at 1087 cm^{-1}, which are coincident with experimental results in Figure 14a. Additionally, we examined the possibility of conversion of trans-NO_2-DR1 to cis-NO_2-DR1 during laser irradiation. The calculated Raman spectra of cis-NO_2-DR1 is quite different from that of amine-DR1 (Figure 14b, lower part), which strongly supports that the peak change arises not from the photoisomerization process (trans-to-cis) but from the photoreduction process (nitro-to-amino groups).

From the Raman spectra of DR1 powder without graphene compared with that on graphene, catalytic effect of graphene can be certified (Figure 16). Whereas the photoreduction of DR1 without graphene slowly occurred, in the case of DR1 on graphene the photoreduction was found to exposure of laser immediately.

The laser focus is also very important due to the power of laser depending on focusing. When the reaction was observed, the focus of irradiated laser at the same position was fixed. As shown Figure 17, when the laser beam was deliberately gone out of focus, the Raman spectra was not changed because the laser power was not enough to cause the reaction of photoreduction. It can be described the change of Raman peak does not come from the difference of laser powers.

We analyzed the change in Raman spectra during the photocatalytic reaction. As shown Figure 18, the photoreductive reaction resulted in the red shift of G peak and blue shift of 2D peak, indicating that graphene is slightly p-doped after the photocatalytic reaction. Furthermore, G peak is sharpening, while 2D peak is broadening.

Further, the experiments were conducted to examine the photoreduction rate depending on the encapsulation of dye molecules by graphene. Figure 19 shows that the photoreduction rate of DR1 adsorbed under graphene is significantly lower than the one on the graphene monolayer. This might be attributed to the gas barrier function of graphene that protects DR1 from exposure to air environment. This means that the source of hydrogen to convert $–NO_2$ to $–NH_2$ groups is from ambient air, which can be further supported by the fact that the dyes sandwiched between two graphene layers show even a slower photoreduction rate. It is difficult to completely exclude other effects. Yet, the difference caused by light absorption might be slight because monolayer graphene almost transmits the incident light, which has only 2.3% of the light absorption. Therefore, in both cases when the molecule was on top of graphene surface and the molecule was under the graphene layer, the effect of graphene as a photoreduction catalyst is similar. In case the encapsulation of dye molecules, although the graphene layer was twice, the molecule was hardly contact with hydrogen as a source of photoreduction because the interaction between graphene layers was strong as though dye molecules was trapped. Thus, the rate of the photoreduction was slow.

In addition, molecules were inserted between graphene two layers to make absence of hydrogen atmosphere. The intercalated molecule between graphene layers was isolated from the air because the interaction between graphene layer was very strong. As this result, it could be supported the photoreductive reaction may occur in a vacuum. In precious reports, Kim *et al.* shown the photo-induced nitro-to-amine conversion occurred in vacuum conditions.[11] They

suggested the possibility of benzene ring as the H-source. For similar reason, it can be estimated hydrogen might come from another molecule as well as air.

As the GERS effect depending on Fermi level of graphene, we also found that increased oxidation of graphene surface by UV/ozone causes increase in photoreduction of dye molecules and controlled reaction rate of photoreduction. It is known that ozone, generated by UV-induced oxygen activation, can be adsorbed onto the graphene surface and the physisorbed molecules can react with graphene surface to form oxygen-containing groups. Consequently, the Fermi level of graphene can be changed and chemical reaction can be tuned. Figure 20 shows a schematic diagram of the graphene Fermi level variation which was treated UV/ozone. For pristine single-layer graphene, the position of the Fermi level is equal to Dirac point. However, when graphene exposed by UV/ozone, the Dirac point will shift below Fermi level due to the p-doping. When the photoreduction occurs on graphene, the electron is easily transferred from graphene to the HOMO level of molecule. Figure 21(a) and (b) are XPS spectra of C 1s peak of pristine graphene and oxidized graphene, respectively. The C ls peak of ozone-oxidized graphene, related to sp^2 C-C bonds, were down-shifted slightly broadened. We also found that the graphene Fermi level is down-shifted by UV/ozone treatment. Figure 21c shows the evolution of the Raman spectra of the graphene surface as a function of UV/ozone exposure time from 0 to 10 min. It is clear that ozone treatment results in the appearance of D peaks, providing evidence for the degree of disorder in graphene structure. The Raman spectra showed a gradual decrease of the intensity and a broadening of the 2D peaks. These results indicate that the surface of graphene was doped by UV/ozone exposure.

Figure 22 shows the Raman spectra of DR1 molecules adsorbed on pristine graphene and oxidized graphene. As mentioned above, the Raman spectra exhibit the clear features of DR1 and also D peaks of graphene. We observed apparent changes in some vibrational bands, especially the peak at 1121 cm^{-1}. This peak, corresponding to ν(N–O) of amino-DR1, increased

gradually on ozone-treated graphene and the catalyst effect of graphene was enhanced after UV/ozone treatment. It is indicated that we can control the catalytic effect of photoreduction by controlling graphene Fermi level (Figure 23).

2.3.4 Conclusion

In summary, we showed that the single layer graphene catalyzes the photoreduction of dye molecules using GERS approaches. We also confirm that graphene-encapsulated nitrobenzene dyes show less photoreduction, implying that the ambient hydrogen molecules are the important source of photoreduction. Our results provide a new understanding on the catalytic function of graphene for adsorbed or intercalated molecular species, where the ultrafast charge-carrier transfer plays a critical role particularly for dye molecules. Thus, we expect that the photocatalytic reactivity of graphene would find numerous energy and environmental applications in the future.

2.3.5 References

1. Zhang, Y.; Tan, Y. -W.; Stormer, H. L.; Kim, P. Experimental observation of the quantum Hall effect and Berry's phase in graphene. *Nature*, **2005**, 438, 201.

2. Novoselov, K. S.; Geim, A. K.; Morozov, S. V.; Jiang, D.; Katsnelson, M. I.; Grigorieva, I. V.; Dubonos S. V.; Firsov, A. A. Two-dimensional gas of massless Dirac fermions in graphene. *Nature*, **2005**, 438, 197-200.

3. Machado, B. F.; Serp, P. Graphene-based materials for catalysis. *Catal. Sci. Technol*., **2012**, 2, 54-57.

4. Ling, X.; Xie, L.; Fang, Y.; Xu, H.; Zhang, H.; Kong, J.; Dresselhaus, M. S. ; Zhang J.; Liu, Z. Can graphene be used as a substrate for Raman enhancement? *Nano Lett*., **2010**, 10, 553-561.

5. Barros, E. B.; Dresselhaus, M. S. Theory of Raman enhancement by two-dimensional materials: Applications for graphene-enhanced Raman spectroscopy. *Phys. Rev. B*, **2014**, 90, 035443.

6. Ling, X.; Moura, L. G.; Pimenta, M. A.; Zhang, J. Charge-Transfer Mechanism in Graphene-Enhanced Raman Scattering *J. Phys. Chem. C*, **2012**, 116, 25112-25118.

7. Loucif-Saibi, R.; Nakatani, K.; Delaire, J. A.; Dumont, M.; Sekkat, Z. Photoisomerization and second harmonic generation in disperse red one-doped and -functionalized poly(methyl methacrylate) films. *Chem. Mater.*, **1993**, 5, 229-236.

8. Marino, I.G. ; Bersani, D. ; Lottici, P.P. ; Tosini, L. ; Montenero, A. Raman investigation of protonation of DR1 molecules in silica or ORMOSILs matrices by the sol-gel technique. *J. Raman Spectrosc*., **2000**, 31, 555-558.

9. Biswas, N.; Umapathy, S. Study of solvent effects on the molecular structure and the reorganization energies of 4-nitro-4′-dimethylaminoazobenzene using resonance Raman intensities. *J. Raman Spectrosc.*, **2001**, 32 (6-7), 471-480.

10. Corma, A.; Concepcio´n, P.; Serna, P. A. Different reaction pathway for the reduction of aromatic nitro compounds on gold catalysts. *Angew. Chem., Int. Ed.*, **2007**, 46, 7266-7269.

11. Kim, K.; Lee, Y. M.; Lee, H. B.; Park, Y.; Bae, T. Y.; Jung, Y. M.; Choi, C. H.; Shin, K. S. Visible laser–induced photoreduction of silver 4-nitrobenzenethiolate revealed by Raman scattering spectroscopy. *J. Raman Spectrosc.*, **2010**, 41, 187-192.

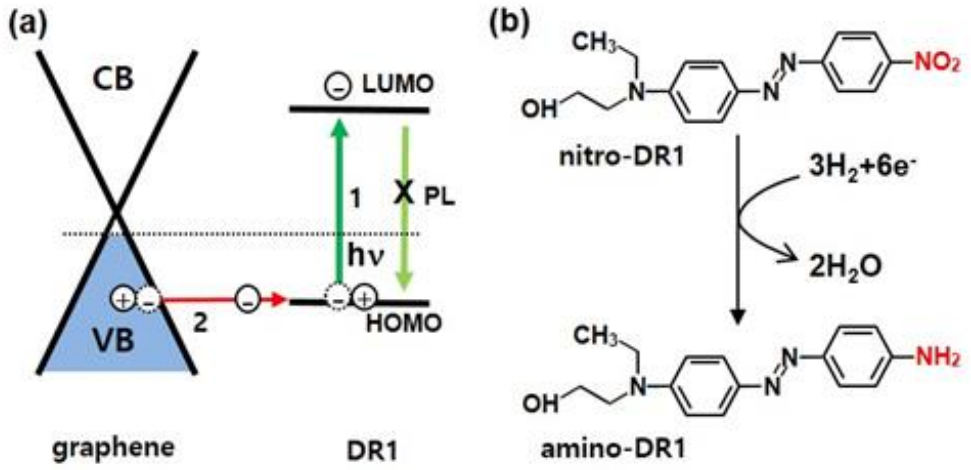

Figure 12. a) Schematic diagram of the graphene-catalyzed photoreduction of DR1. (b) Molecular structures of nitro/amino-DR1.

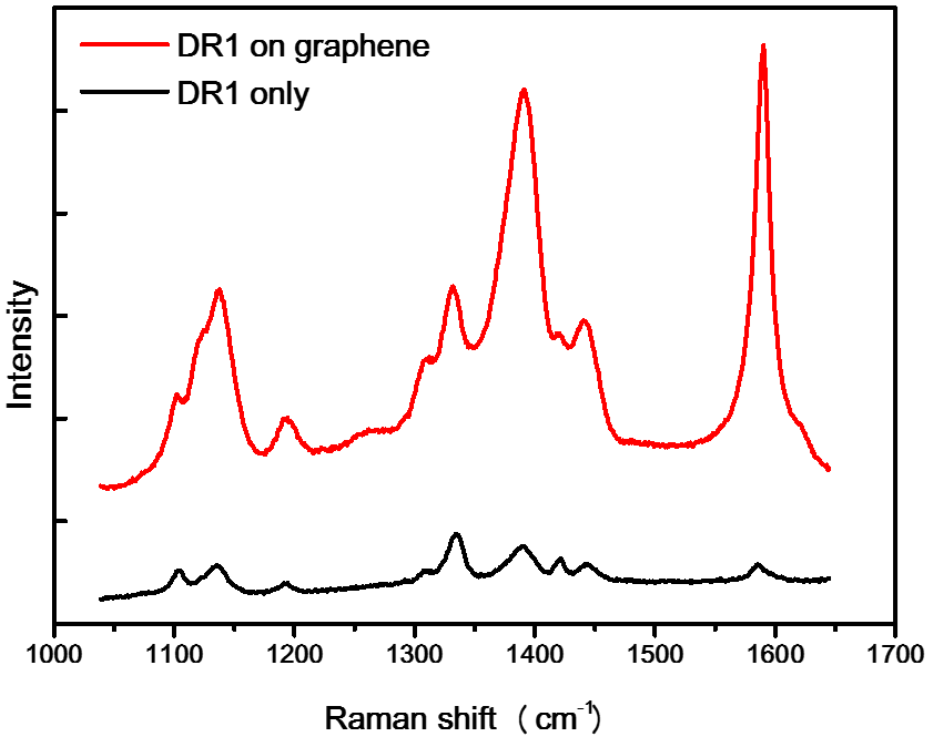

Figure 13. Raman spectra of DR1 on graphene (red) and without graphene (black).

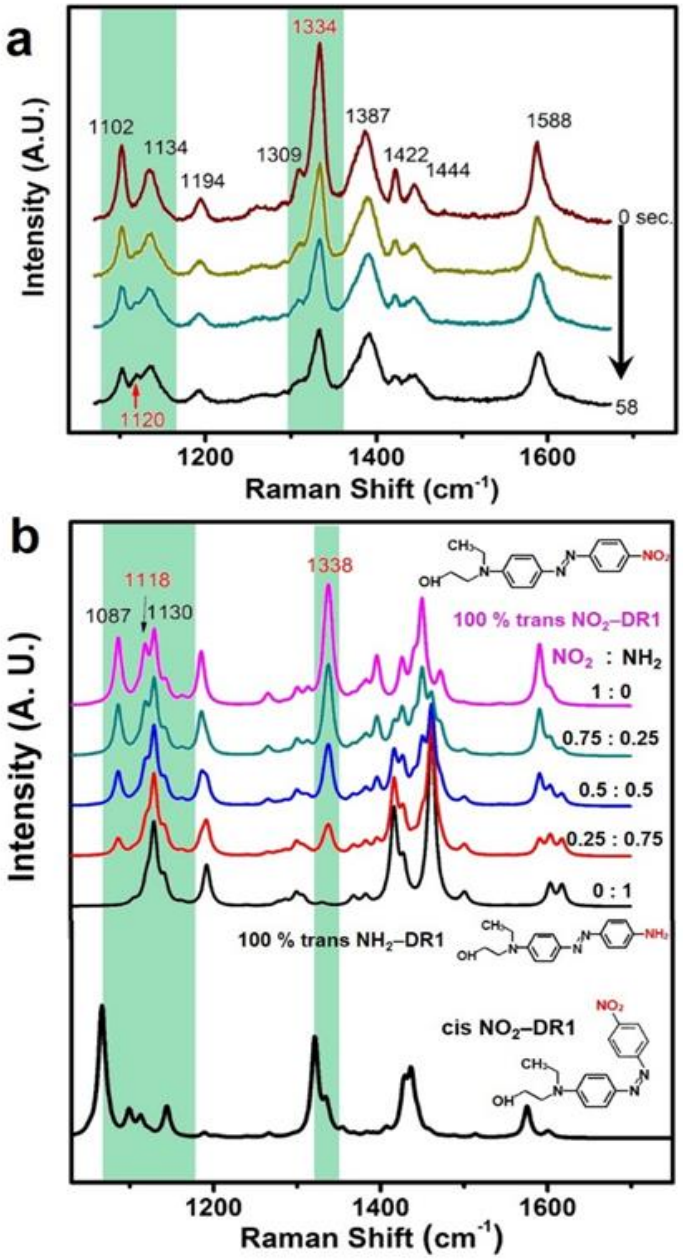

Figure 14. (a) Time evolution of Raman spectra of DR1 adsorbed on a single layer graphene. Laser excitation wavelength, 514.5 nm. (b) Simulated Raman spectra of trans-NO_2-DR1, trans-NH_2-DR1, and cis-NO_2-DR1 calculated by a DFT method (B3LYP- 6-31G (d,p)).

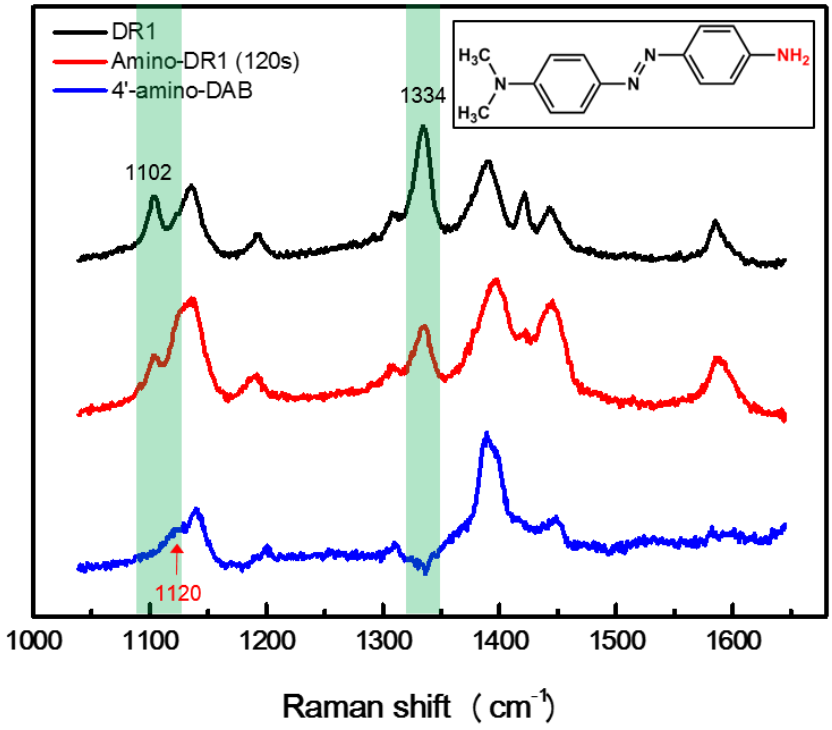

Figure 15. Normal Raman Spectra of nitro-DR1, amino-DR1 (after exposure to laser for 120 sec) and 4'-amino-DAB. (Inset) The molecule structure of 4'-amino-DAB.

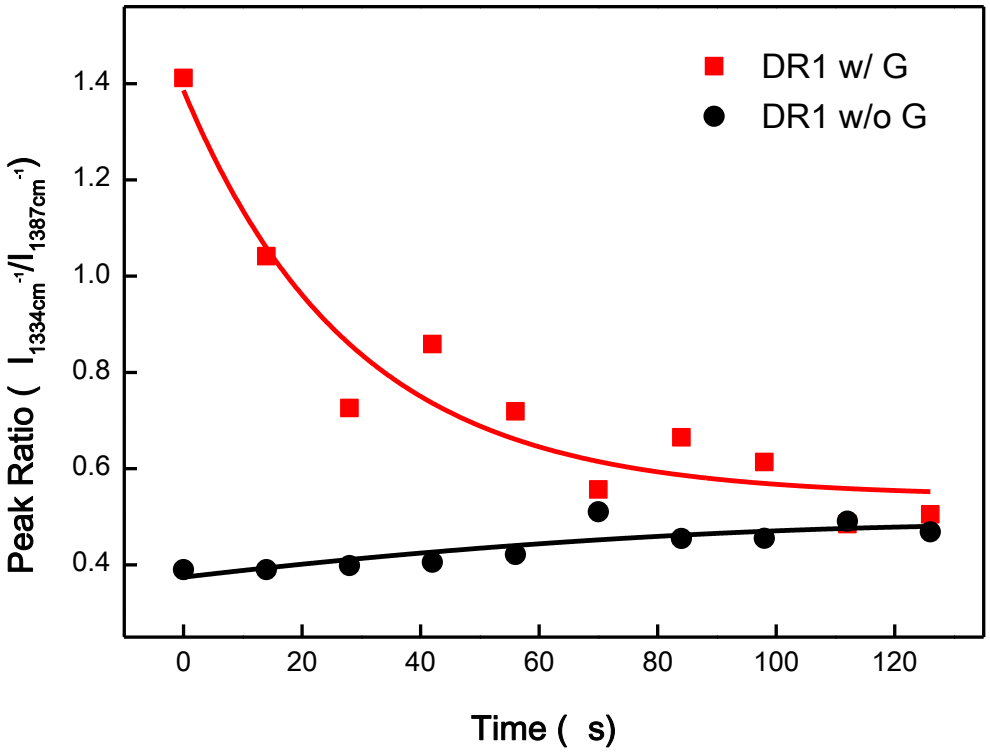

Figure 16. Photoreduction rate of DR1 without graphene compared to that on graphene.

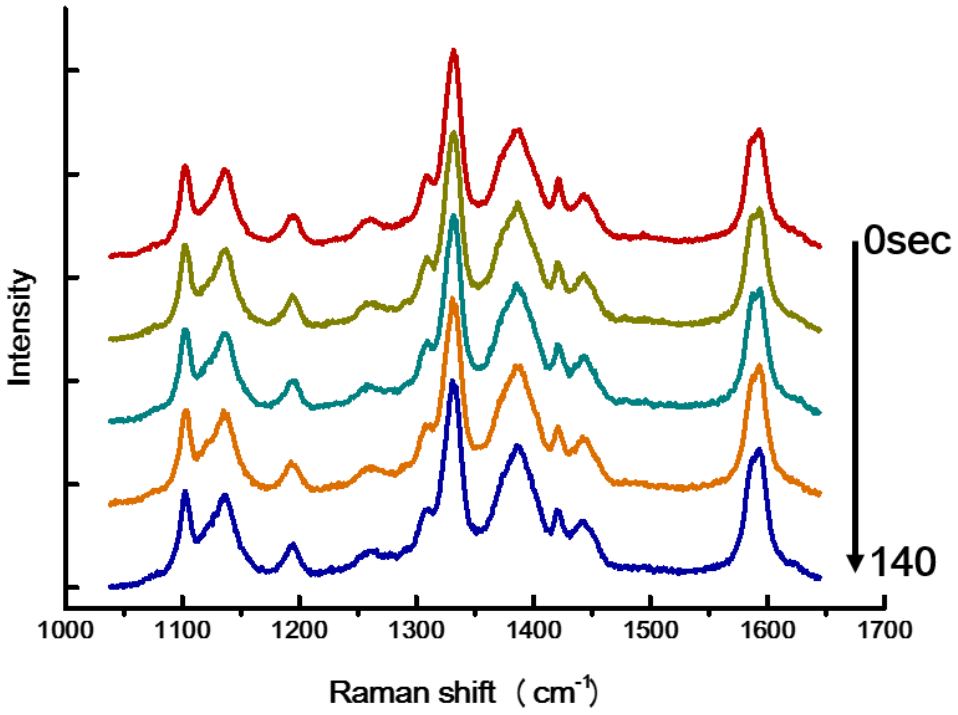

Figure 17. Time evolution of Raman Spectra of DR1 adsorbed on graphene by defocused laser.

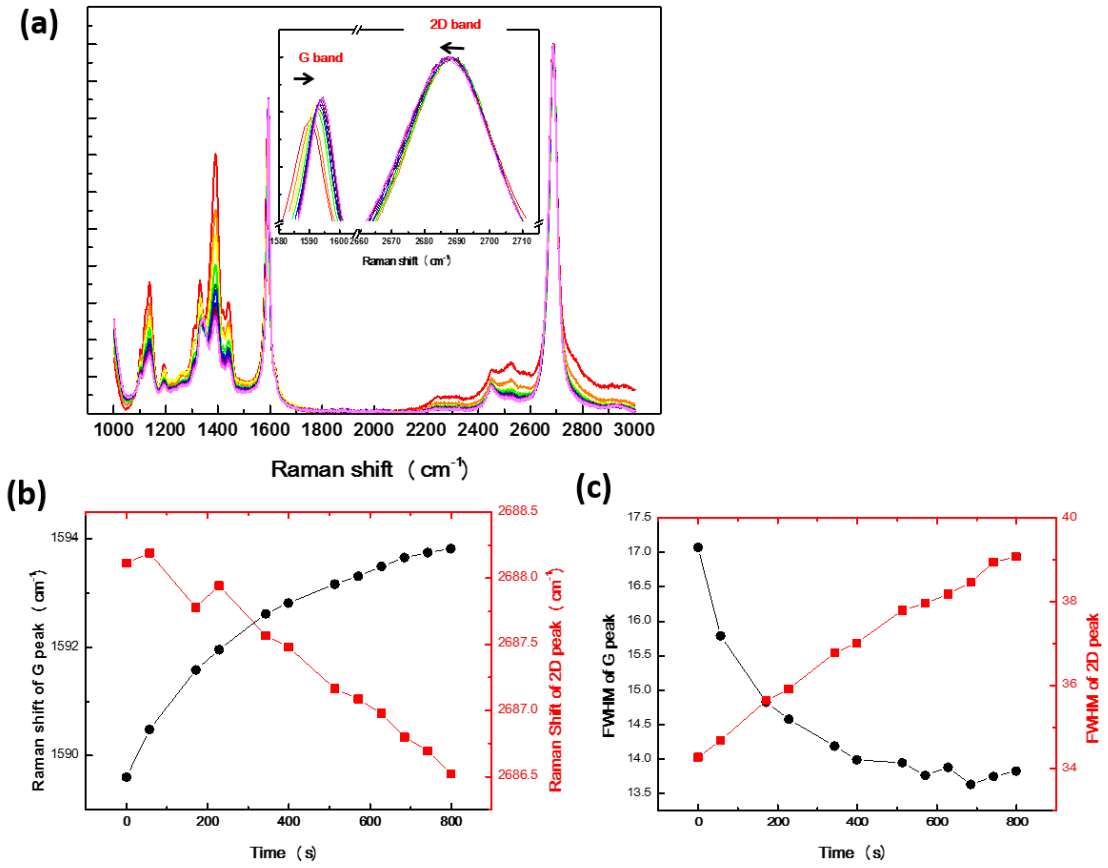

Figure 18. (a) Change in Raman spectra of DR1 on graphene with increasing laser irradiation time. The inset shows the magnified plots of G and 2D band peaks related to graphene. Time dependent change in Raman G and 2D peak positions and full width at half maximum (FWHM) are shown in (b) and (c), respectively.

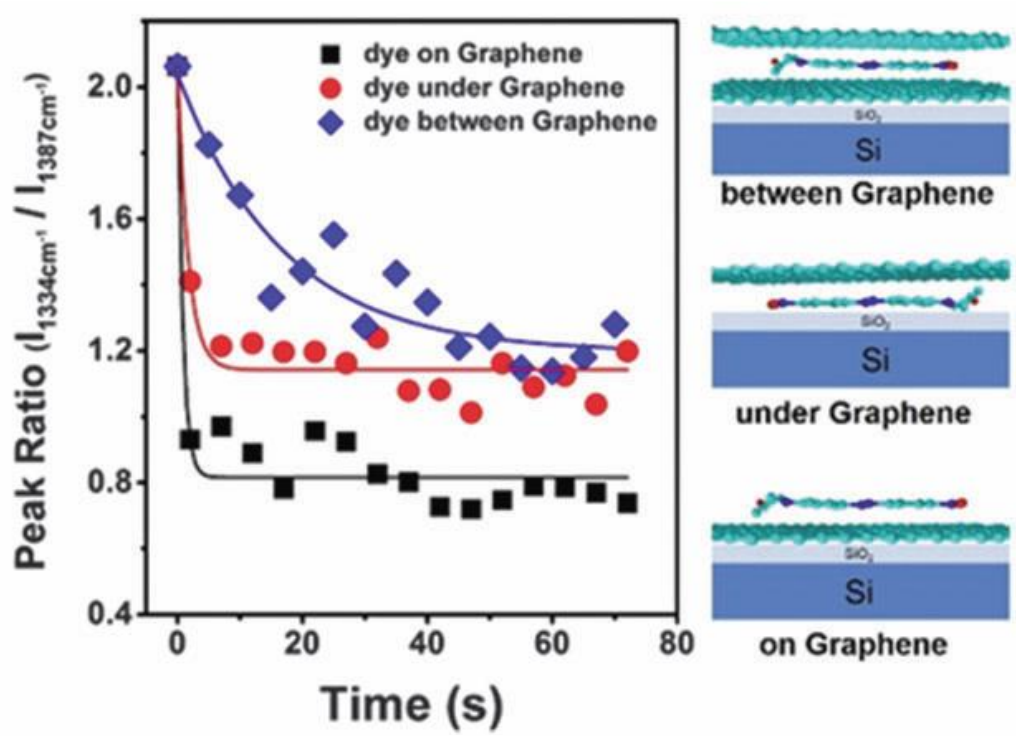

Figure 19. Graphene-encapsulated nitrobenzene dyes show less photoreduction, implying that the ambient hydrogen molecules are the importance source of photoreduction.

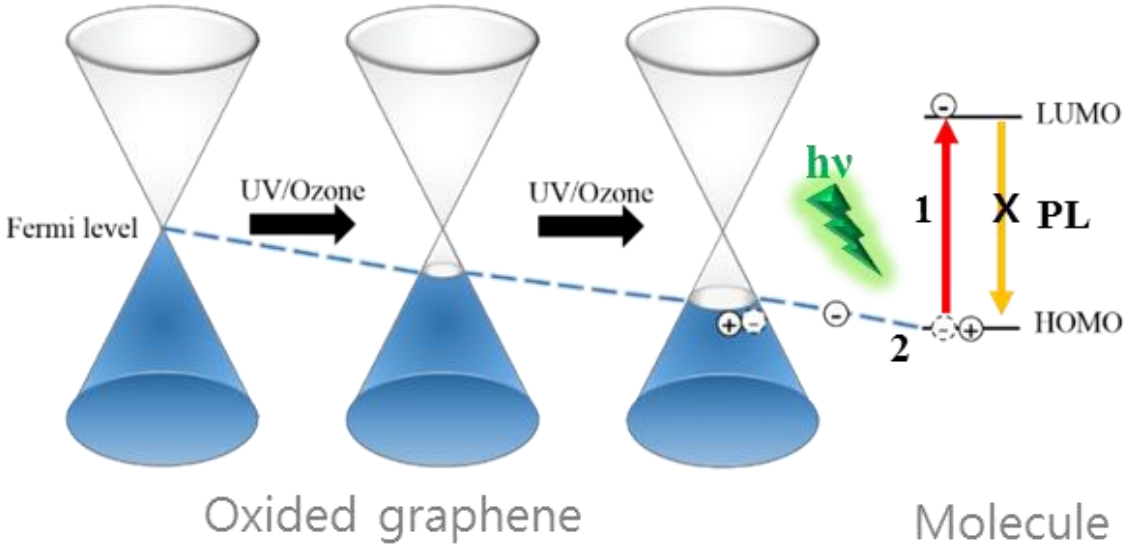

Figure 20. Schematic diagram of the graphene Fermi level variation which was treated UV/ozone.

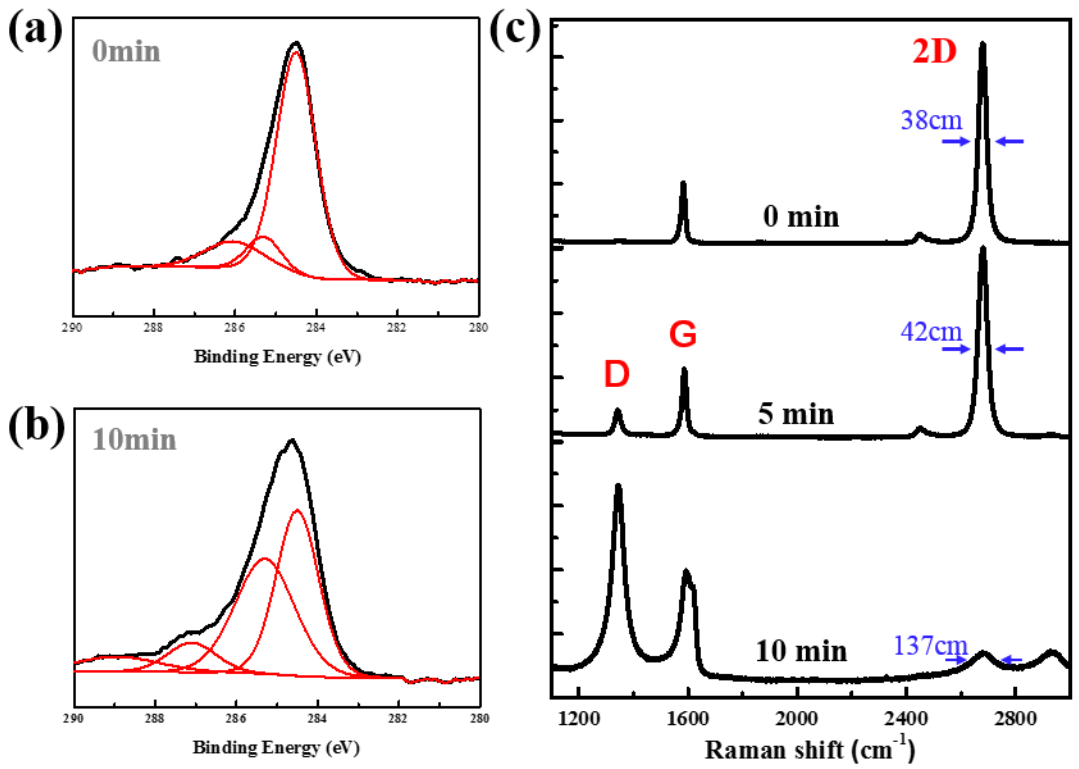

Figure 21. XPS spectra of pristine graphene (a) and oxidized graphene by treating ozone for 10 minutes. (c) shows the evolution of the Raman spectra of the graphene surface as a function of UV/ozone exposure time from 0 to 10 min.

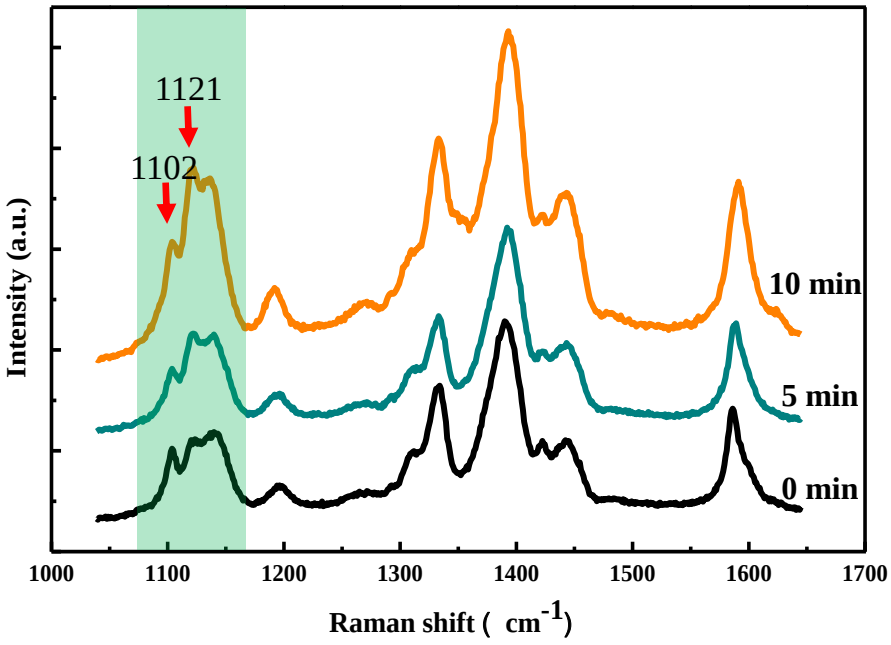

Figure 22. Raman spectra of DR1 adsorbed onto pristine graphene (0 min) and ozone-treated graphene for 5 and 10 min.

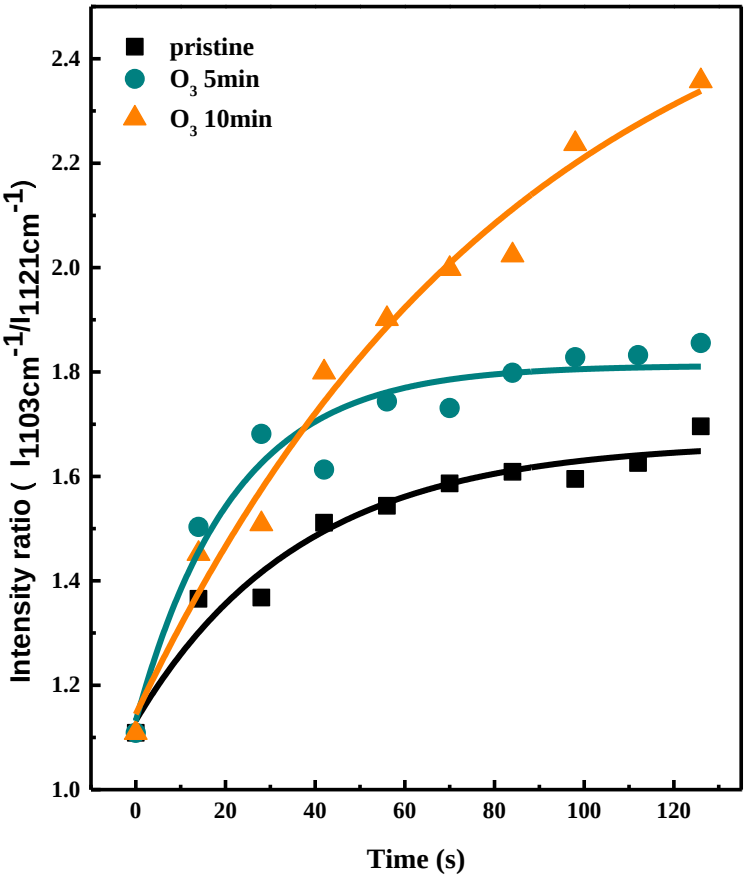

Figure 23. Photoreduction rate of DR1 adsorbed onto pristine graphene and ozone-treated graphene for 5 and 10 min.

Chapter 3. Enhanced DNA Sensing by Surface-Passivated Graphene

3.1 Introduction

Graphene-DNA Hybrid. Among the various biomolecules, DNA emerged as a new class of material, which is an interesting synthetic building block to generate nanoscale architectures and assemblies of nanomaterials. Further, DNA has been exploited as a potential material in different fields and most of the applications are acquired based on combining DNA with other chemicals, particularly nanomaterials by different interactions.[1,2] DNA consists of on long polymer of simple units called nucleotides, with the nucleobases such as adenine (A), guanine (G), cytosine (C), and thymine (T) with backbones made of sugars (deoxyribose) and phosphate groups connected through ester bonds. The double stranded DNA (dsDNA) is stabilized or held together by hydrogen bonding between the bases linked (Figure 1)[2].

Since graphene have large surface area (up to 2630m^2/g)[3] and unique sp^2-bonded structure, have been widely used to selectively enrich and detect aromatic molecules and single-stranded DNA (ssDNA) through a hydrophobic force and π-π stacking interactions.[4,5,6] While graphene is a hydrophobic material, graphene oxide (GO) is high solubility in water by generating surface carboxylic acid and hydroxyl groups. It is widely used in biosensors and bioimaging because of its high fluorescence quenching efficiency, facile chemical conjugation, unique amphiphile property, and low cost.[7,8] Such applications are possible because of two unique properties of GO: 1) the strong binding to ssDNA with a high affinity, while the affinity for dsDNA is much lower; 2) a universal fluorescence quencher, many organic dyes and quantum dots can be effectively quenched by GO. With these properties, sensitive fluorescent sensors with a high signal-to-noise ratio can be constructed using GO and DNA.

Graphene-Based Fluorescent Biosensor. The well-known application of graphene in biosensor technology is fluorescent detection because graphene is a good energy acceptor in fluorescence resonance energy transfer (FRET), which is known to be a sensitive and reliable analytical method, is widely used in biological analysis.

In a typical method, fluorescent dye-labeled ssDNA was adsorbed on surface of graphene via π-π stacking interaction, by which the fluorescence of dye was completely quenched due to FRET. In the presence of a target, the fluorescence-quenching effect can be significantly inhibited when the ssDNA was hybridized with its complementary target DNA to form dsDNA. The availability of nucleobases to the basal plane of graphene was reduced due to the restriction of nucleobases between the densely negative-charged helical phosphate backbones, causing the weak interaction between dsDNA and graphene surface.

Although practical applications of GO in bioanalysis have been demonstrated, the interaction between DNA and GO has not been fully investigated. In *Liu* groups, the adsorption and desorption of fluorescent-labeled DNA on GO surface have been examined as functions of DNA length, pH, and salt. Desorption can occur by adding the complementary DNA to form dsDNA, adding the same DNA to exchange (figure 2a).[9] In addition, DNA-length-dependent fluorescence quenching within a few nanometers from the GO was investigated by using covalently linked probes to a GO (figure 2b).[10] In the same group, a remarkable surface reaction mechanisms of DNA on GO has been proposed, in which the GO-pre-adsorbed probe DNA is nonspecifically displaced by incoming DNAs.[11] Further, Park *et al*. investigated desorption of ssDNA from the GO surface using either complementary or non-complementary ssDNA to compare the desorption efficiency of base-paired duplex DNA with that of simple nonspecific displacement of adsorbed ssDNA from GO. They also analyzed the dissociation kinetics of

ssDNA adsorbed on GO surface by adding complementary or non-complementary strand DNAs.[12]

3.2 Experimental

Graphene Oxide Synthesis. The GO flakes were prepared by the Hummers method[13, 14] with minor modification. Briefly, 5 g graphite (99.9995 %, Alfa Aesar) was put into 169 mL sulphuric acid (95 %, H_2SO_4, Samchun Chemicals), followed by adding 3.8 g sodium nitrate ($NaNO_3$, Sigma Aldrich). After mixing completely, potassium permanganate ($KMnO_4$, Sigma Aldrich), the oxidative reagent, was slowly poured (22.5 g over 3 hours) into the mixed solution with stirring in ice bath to keep the solution temperature at < 10 °C, followed by storing in ambient condition for 5 days. After reaction, 15 mL hydrogen peroxide (H_2O_2, 30 – 35.5 %, Samchum Chemicals) was added into the mixed solution, and the solution was mildly stirred for 1 day. For purification, distilled water was added into the reaction solution, followed by centrifugation at 5000 rpm for 30 minutes and removing the supernatant liquid of the solution. The rinsing was repeated more than a dozen or so times in order to eliminate the salt residues and acid completely. Finally, the GO flakes were dried in a desiccator for modification.

Sample Preparation. All DNA oligonucleotides were purchased from Bioneer Co. (Korea). The sequences of DNA samples are as follows: the dye-labeled probe DNA is 5'-FAM-TCTCAACTCGTA-3' (FAM = fluorescein-based dye), the complementary target DNA sequence is 5'-TACGAGTTGAGA-3', the mismatch DNA sequence is 5'-TAC**C**A**C**T**A**GAGA-3' (mismatch are shown in bold type), and passivation DNA is 5'-AGGTCGCCGCCC-3'. The concentration of FAM-labeled probe DNA were 50nM, that of target DNA or mismatched DNA is different concentrations (5, 10, 15, 20, 25, 35, 50, 100, and 200 nM) in the PBS buffer (100 nM NaCl, 10nM PB, 10 mM $MgCl_2$, pH 7.4), and the passivation DNA used with a concentration of 10μM.

50 nM of FAM-probe ssDNA was mixed with GO (10μg/ml) in a PBS buffer. After passivation ssDNA and target or mismatch DNA were sequentially added to the solution of

probe DNA-GO complex, fluorescence measurements were performed. Each step was incubated at room temperature for 1 hour to allow sufficiently complex formation.

Characterization. Fluorescence profiles were measured by a SynergyMx multi-mode reader (BioTek Inc.) with excitation at 492nm and emission range from 490 to 600nm.

3.3 Results and Discussion

As demonstrated previous reports, in graphene based fluorescent DNA sensor, the added cDNA might compete with the adsorbed probe DNA nonspecifically for surface binding sites due to bind between graphene and probe DNA *via* π- π stacking interaction and van der Waals force. Some of the probe DNA might be displaced by the cDNA into the solution phase to hybridize with the free cDNA (see the figure 2c)[12]. These reactions could consequentially cause to reduce the sensitivity of sensor and obscure detailed quantitative analysis.

Herein, to prevent undesired reaction, we proposed "passivation method" of probe DNA-GO complex. Figure 3 is a brief scheme of process. As mentioned above, GO could absorb dye-labeled ssDNA via van der Waals force between nucleobases and the basal plane of GO, by which the fluorescence of the dye was quenched. Afterwards, the fluorescence-quenching effect can be significantly inhibited when the ssDNA was hybridized with its complementary target DNA to form dsDNA. The availability of nucleobases to the basal plane of GO was substantially reduced due to the restriction of nucleobases between the densely negative-charged phosphate backbone, causing the weak affinity to GO and subsequent retention of the fluorescence.

Figure 4 shows the fluorescence intensity decreased with increased concentration of graphene oxide due to strong charge-transfer interaction. It shows also the fluorescence of GO and buffer solution as references. In our experiment, 10μg/ml was chosen the as optimized GO concentration because over 90% fluorescence was quenched.

As previous research, when probe DNA was preadsorbed on GO, the addition of noncomplementary ssDNA led to an increase in fluorescence.[11] Similarly, when passivation DNA was added into probe DNA-GO complex, the fluorescence intensity was re-emerged

(Figure 5). Thus, all fluorescence intensities were relatively represented to revise the fluorescence generated by passivation (see shown Figure 6).

Figure 6 displays that relative fluorescence intensity of dye-labeled probe DNA at various concentrations of cDNA (a, b) or mDNA (c, d). In the case of the surface of probe DNA-GO complex covered with an excess of passivation DNA, which has random sequence, fluorescence recovery was observed at low concentration (Figure 6b, 6d) rather than the complex without passivation. To clarify the effect of passivation, we replotted fluorescence at 517nm in Figure 6 (Figure 7). The x-axis is log value of concentration of cDNA or mDNA. As shown this figure, the recovery of fluorescence depending on incoming ssDNA has a linear relationship after passivating on the surface of graphene.

We can also calculate the limit of detection (LOD, defined as LOD = 3.3*(standard deviation of the response (σ)/slope of the calibration curve (S))) from these data. In the case of passivation, it has a lower LOD of 2.04nM compared to the value when it is not (3.30nM).

On the basis of these results, by passivating on the surface of GO, we can minimize nonspecific adsorption of incoming DNA and enhance the sensitivity and the selectivity of DNA sensor.

3.4 Conclusion

The fluorescence intensity of probe DNA with FAM can be sharply quenched by addition of graphene oxide. The overall trend was that the higher concentration of c-/m-DNA, the higher the fluorescence intensity, suggesting that the complementary DNA can be formed double-helix and the mismatched DNA was partially hybridization. We demonstrated that passivating the uncovered GO surface with additional DNAs whose sequence is different from that of probe/c/m-DNAs substantially increase the sensitivity and selectivity of DNA sensing, which is more effective at lower concentration. This is because the non-interacting DNAs densely packed on GO surface prevent the unexpected binding of c/m-DNAs with GO, and selectively allow the double-helix formation between probe-DNA and c/m-DNAs.

3.5 References

1. Kwon, Y. W.; Lee, C. H.; Choi, D. H.; Jin, J. I. Materials science of DNA. *Mater. Chem.* **2009**, 19, 1353–1380.

2. Premkumar, T.; Geckeler, K. E. Graphene–DNA hybrid materials: Assembly, applications, and prospects. *Progress in Polyer Science* **2012**, 37, 515-529.

3. Zhu, Y.; Murali, S.; Cai, W.; Li, X.; Suk, J.W.; Potts, J.R.; Ruoff, R.S. Graphene and graphene oxide: synthesis, properties, and applications. *Adv. Mater.* **2010**, 22 (35), 3906-3924.

4. Liu, Z.; Robinson, J. T.; Sun, X.; Dai, H. PEGylated Nanographene Oxide for Delivery of Water-Insoluble Cancer Drugs. *J. Am. Chem. Soc.* **2008**, 130 (33), 10876-10877.

5. Sun, X.; Zhang, Y.; Zhang, X.; Yu, J.; Li, Y.; Yang, X.; Dai, Z.; Li, M. Nano-Graphene Oxide for Cellular Imaging and Drug Delivery. *Nano Res.*, **2008**, 1 (3), 203-206.

6. Tang, Z.; Wu, H.; Cort, J. R.; Buchko, G. W.; Zhang, Y.; Shao, Y.; Aksay, I. A.; Liu, J.; Lin, Y. Constraint of DNA on Functionalized Graphene Improves its Biostability and Specificity. *Small* **2010**, 6 (11), 1205-1209.

7. Liu, X. Q.; Wang, F.; Aizen, R.; Yehezkeli, O.; Willner, I. Graphene Oxide/Nucleic-Acid-Stabilized Silver Nanoclusters: Functional Hybrid Materials for Optical Aptamer Sensing and Multiplexed Analysis of Pathogenic DNAs. *J. Am. Chem. Soc.* **2013**, 135 (32), 11832-11839.

8. Zhu, Y. W.; Murali, S.; Cai, W. W.; Li, X. S.; Suk, J. W.; Potts, J. R.; Ruoff, R. S. Graphene and graphene oxide: synthesis, properties, and applications. *Adv. Mater.* **2010**, 22, 3906-3924.

9. Wu, M.; Kempaiah, R.; Huang, P.-J. J.; Maheshwari, V.; Liu, J. Adsorption and desorption of DNA on graphene oxide studied by fluorescently labeled oligonucleotides. *Langmuir* **2011**, 27, 2731-2738.

10. Huang, P.-J. J.; Liu, J. DNA-Length-Dependent Fluorescence Signaling on Graphene Oxide Surface. *Small* **2012**, 8 (7), 977-983.

11. Park, J. S.; Goo, N.-I.; Kim, D.-E. Mechanism of DNA Adsorption and Desorption on. Graphene Oxide. *Langmuir* **2014**, 30, 12587-12595.

12. Liu, B.; Sun, Z.; Zhang, X.; Liu, J. Mechanisms of DNA Sensing on Graphene Oxide. *Anal. Chem.* **2013**, 85, 7987-7993.

13. Hummers, W. S.; Offeman, R. E. Preparation of graphitic oxide. *J. Am. Chem. Soc.* **1958**, 80, 1339.

14. Marcano, D. C.; Kosynkin, D. V.; Berlin, J. M.; Sinitskii, A.; Sun, Z.; Slesarev, A.; Alemany, L. B.; Lu, W.; Tour, J. M. Improved Synthesis of Graphene Oxide. *ACS Nano* **2010**, 4 (8), 4806-4814.

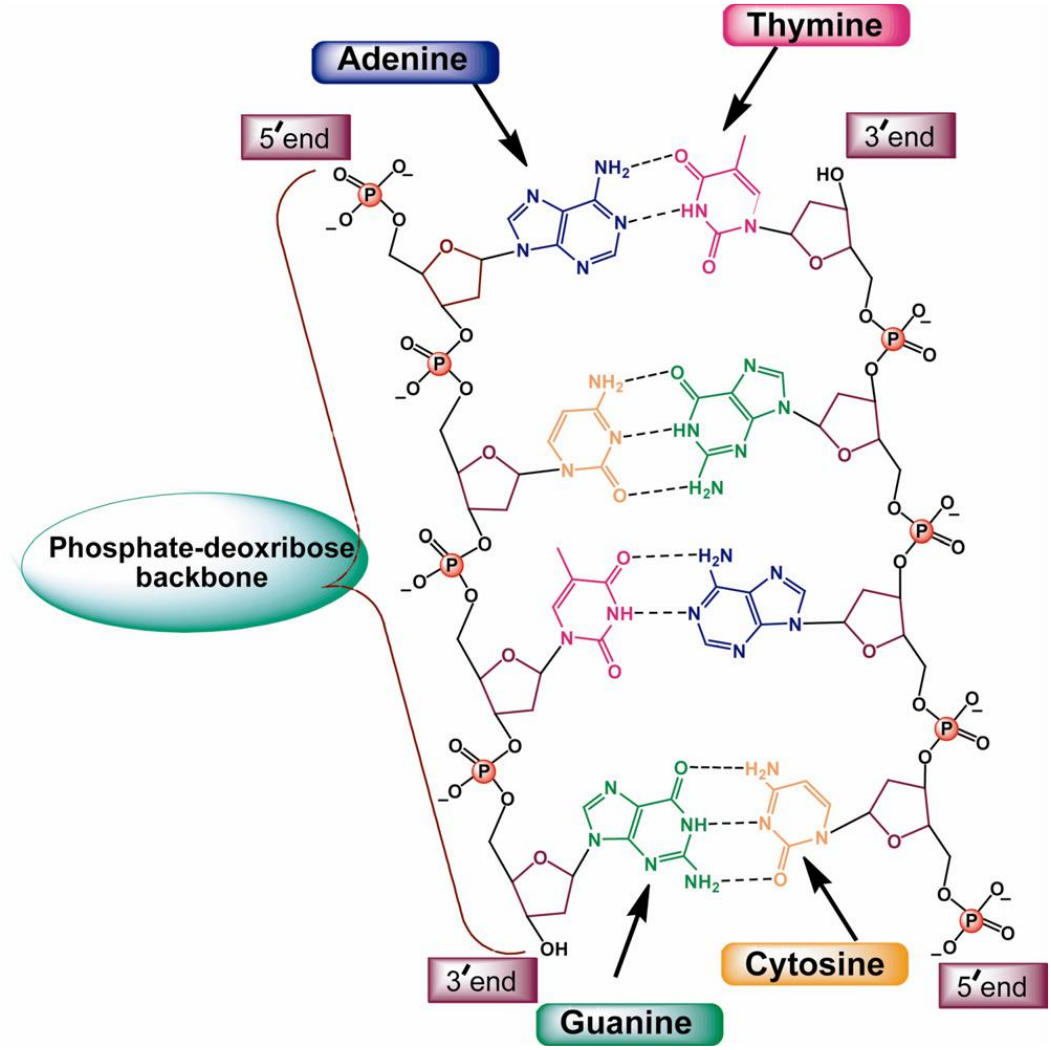

Figure 1. Chemical structure of DNA. Dotted lines shown are hydrogen bonds between the bases.[2]

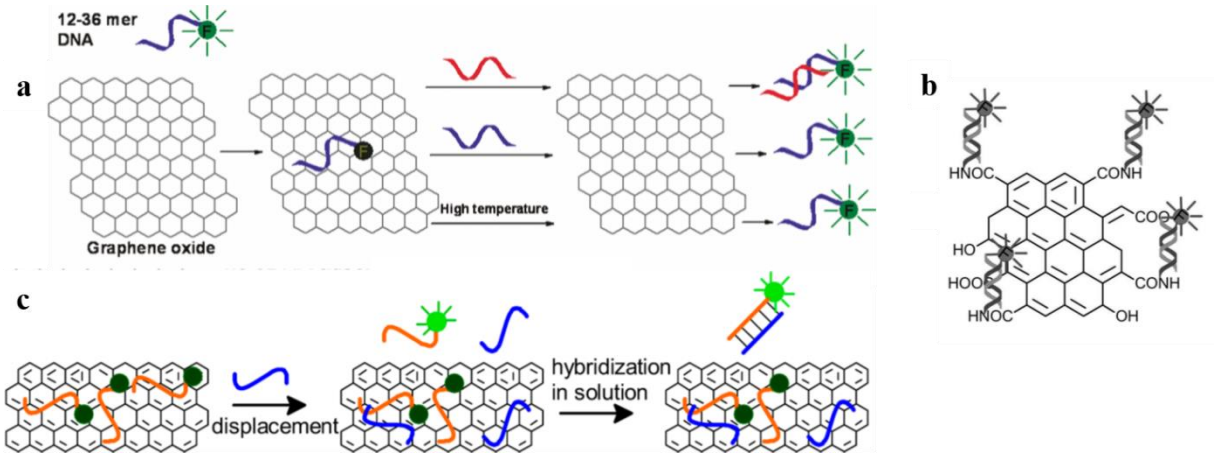

Figure 2. (a) Scheme of FAM-labeled DNA adsorption and desorption on GO. Fluorescence is quenched upon adsorption. Desorption can be achieved by adding the c-DNA (reaction 1), DNA exchange with the same DNA (reaction 2), or increasing temperature (reaction 3).[9] (b) Schematics of covalently linked probes with GO. The fluorescence properties of the GO samples containing only covalently attached DNAs were analyzed. (c) Displacement mechanism of hybridization between a probe DNA adsorbed by GO and its cDNA (target DNA). The oxygenated groups and defeats on GO are omitted. In the case, the probe DNA with a fluorophore label is preadsorbed and the cDNA is added afterward. The tendency of GO adsorbing dsDNA is lower than that of the adsorption of ssDNA.

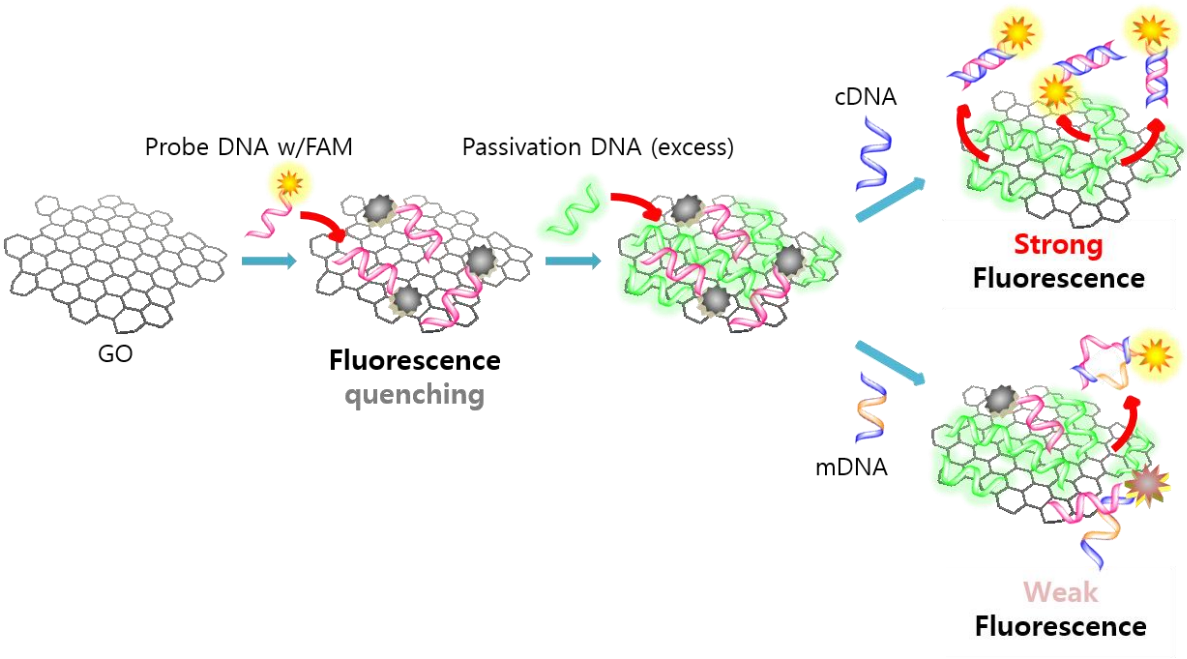

Figure 3. Schematic presentation of the DNA-GO complex through passivation method.

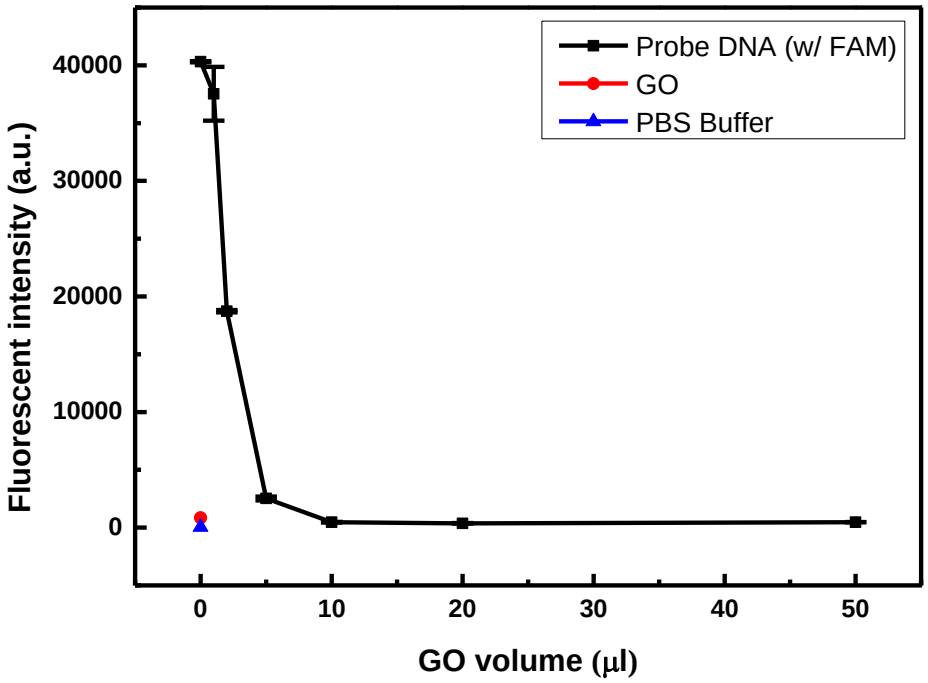

Figure 4. Fluorescence intensity of probe DNA with FAM as the volume of GO and reference (only GO, buffer).

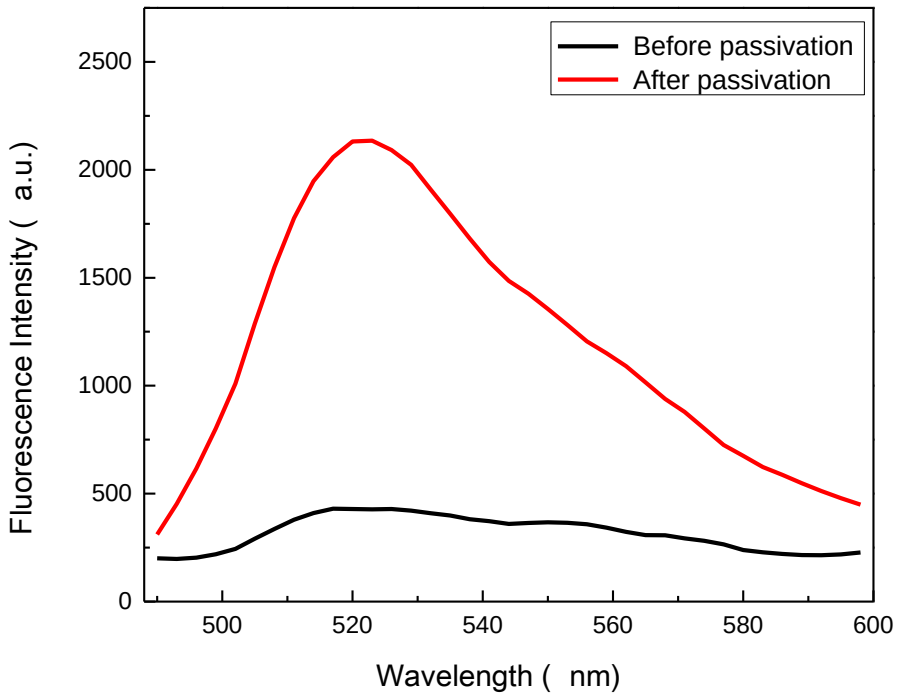

Figure 5. The fluorescence spectrum of dye-labeled DNA-GO complex (black line) and the mixture of DNA-GO complex and passivation DNA (red line). When passivation DNA was added, fluorescence was revealed.

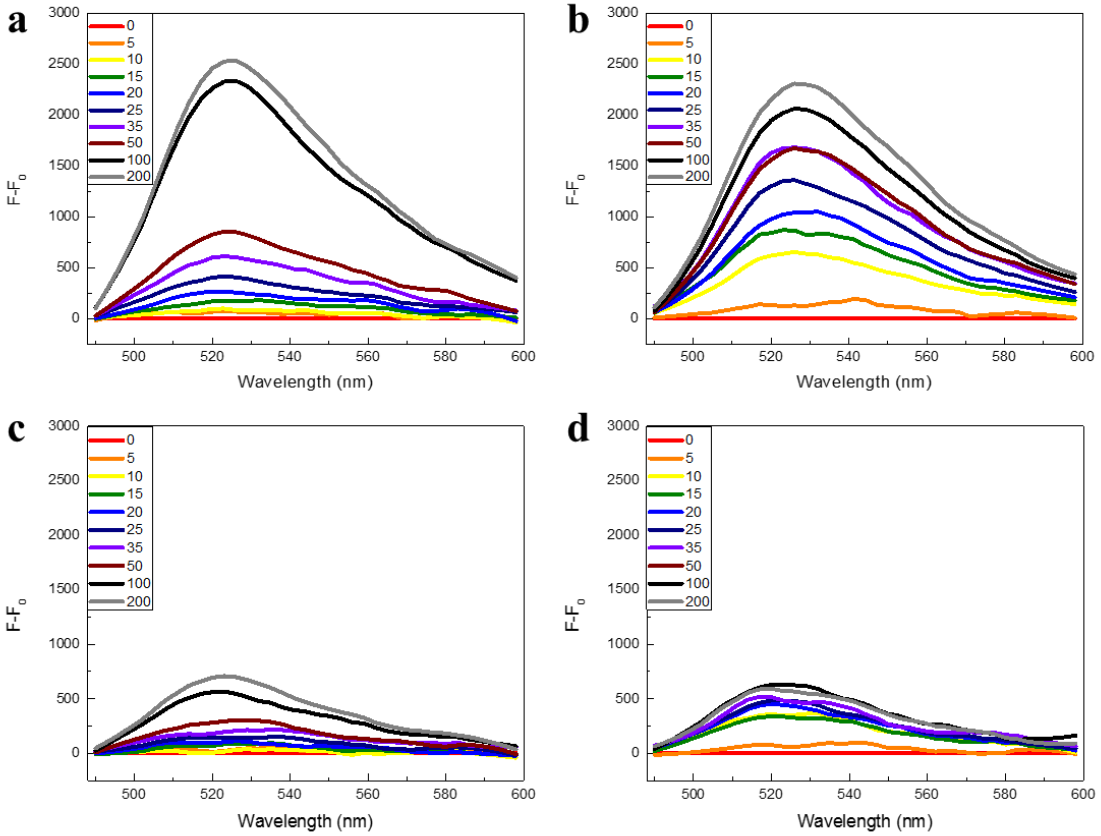

Figure 6. The relative fluorescence spectra at various concentrations of complementary DNA (a, b) or mismatched DNA (c, d). (a) and (c) are not passivated on surface of GO, while (b) and (d) are passivated on surface of GO.

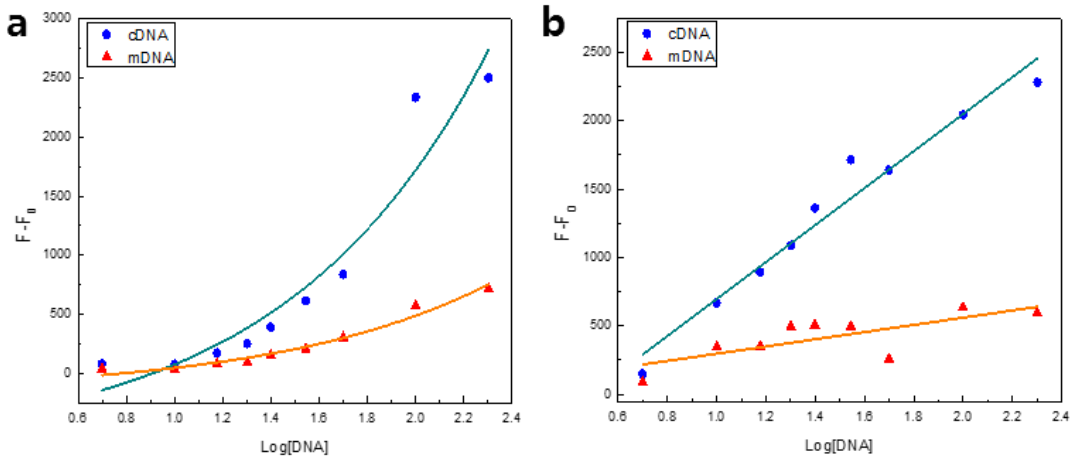

Figure 7. The relative fluorescence of dye-labeled probe DNA at 517nm with log value of concentration of c/m-DNA. It is replotted data in figure 6. It is indicated that the recovery of fluorescence without (a) and with (b) passivation on surface of graphene oxide.

Appendix

A. List of Publication

B. List of Presentation

A. List of Publications

1. **Lee, B**.; Kang, J. H.; Jo, I.; Shin, D.; Hong, B. H. Graphene-Catalyzed Photoreduction of Dye Molecules Revealed by Graphene Enhanced Raman Spectroscopy. *Phys. Chem. Chem. Phys.* **2016**, 19, 3413-3415.

2. Yu, S. –H.; **Lee, B.**; Choi, S.; Park, S.; Hong, B. H.; Sung, Y. –E. Enhancement of electrochemical properties by polysulfide trap in graphene-coated sulfur cathode on patterned current collector. *Chem. Commun.* **2016**, 52, 3203-3206.
   (co-first authorship)

3. Shin, D.; Park, J. B.; Kim, Y. –J.; Kim, S. J.; Kang, J. H.; **Lee, B.**; Cho, S. –P.; Hong, B. H., Growth Dynamics and Gas Transport Mechanism of Nanobubbles in Graphene Liquid Cells. *Nat. Commun*. **2015**, 6, 6068.

4. Kim, S. J.; Choi, T.; **Lee, B**.; Lee, S.; Choi, K.; Park, J. B.; Yoo, J. M.; Choi, Y. S.; Ryu, J.; Kim, P.; Hone, J.; Hong, B. H., Ultraclean Patterned Transfer of Single-Layer Graphene by Recyclable Pressure Sensitive Adhesive Films. *Nano Lett.* **2015**, 15, 3236-3240.

5. Kim, S. J.; Choi, K.; **Lee, B**.; Kim, Y.; Hong, B. H., Materials for Flexible, Stretchable Electronics: Graphene and 2D Materials. *Ann. Rev. Mater. Res*. **2015**, 45, 63-84.

6. Kim, Y. –J.; Kim, S. J.; Jung, M. H.; Choi, K. Y.; Bae, S.; Lee, S. –K.; Lee, Y.; Shin, D.; **Lee, B.**; Shin, H.; Choi, M.; Park, K.; Ahn, J. –H.; Hong, B. H., Low temperature growth and direct transfer of graphene–graphitic carbon films on flexible plastic substrates. *Nanotechnology*, **2012**, 23, 344016.

B. List of Presentations

1. Lee, B.; Kang, J. H.; Jo, I.; Shin, D.; Hong, B. H.; Graphene-catalyzed Photoreduction of Dye Molecules Revealed by Graphene Enhanced Raman Spectroscopy, The 3rd Graphene Symposium, Korea, Apr. 2016.

2. Lee, B.; Lee, M.; Kim, Y. –G.; Hong, B. H.; Highly Sensitive and Selective DNA Sensing by Surface-passivated Graphene, Graphene Week 2015, UK, Jun. 2015.

3. Lee, B.; Lee, M.; Kim, Y. –G.; Hong, B. H.; Highly Sensitive and Selective DNA Sensing by Surface-passivated Graphene, The 1st International Conference on 2D Materials, China, Oct. 2014.

5. Lee, B.; Lee, M.; Kim, Y. –G.; Hong, B. H.; Highly Sensitive and Selective DNA Sensing by Surface-passivated Graphene, 2013 SNU-HU Chemistry Symposium, Korea, Dec. 2013.

6. **Lee, B.**; Kim, K. E.; Bae, S.; Hong, B. H.; Properties of Grpahene Films Depending on Etching, Nano Korea, Korea, Aug. 2011.

요약 (국문초록)

1장에서는 이 논문에서 기본적인 지식에 대해 기술한다. 그래핀의 합성 방법과 특성에 대해 간략히 소개하였다.

그래핀의 여러 응용 분야 중에 라만을 이용한 그래핀-표면 증강 산란 (Graphene-Enhanced Raman Spectroscopy, GERS)이 있다. 이는 그래핀의 전하 이동도가 매우 빨라 형광을 소광시키는 그래핀의 특성에서 기인한 것이며, 이로 인하여 그래핀 위에서 라만 신호가 상당히 증가되는 현상이다. 그러나, GERS 및 형광 신호 소광에 대한 기본 메커니즘은 아직 명확하게 증명되지 않았다.

2장에서는 GERS에 대한 메커니즘 연구 및 이를 기반으로 한 광환원 반응 응용 연구를 설명한다. 2. 2장에서는 그래핀 두 장을 적층한 샌드위치 구조물의 라만 산란 특성 연구를 소개하였는데, 라만 산란 특성이 그래핀 사이에 있는 분자 구조가 평면인지 아닌지에 따라 다르게 나타난다. 두 그래핀 층 사이에 존재하는 평면 염료 분자의 경우, 그 분자가 가지는 흡광도와 주사한 레이저 파장의 중첩에 따라 라만 신호 증감이 일어난다. 이 반응은 일반적으로 알려진 라만 향상 메커니즘을 따른다. 한편, 비평면 염료 분자에서는, 라만 신호 증감이 비일반적으로 나타나게 되는데, 이는 비평면 염료 분자에 의해 생긴 양자 공극 공간에 의해 생성된 새로운 에너지 상태와의 공명에 기인한다고 여겨진다. 이러한 결과는 GERS의 메커니즘에 대한 더 깊은 이해를 도울 뿐만 아니라 다양한 화학 및 생물학적 연구에서 그래핀 샌드위치 구조가 보다 민감하고 견고한 분석 플랫폼이 될 것을 제시한다.

2.3 장에서 그래핀을 이용한 표면 증강 라만 분광을 통하여 단일 층 그래핀은 그 자체로 분자의 광환원 반응에 촉매로 이용 가능함을 보였다. 라만 레이저에 의해 분자의 전자가 들뜨게 되면 분자의 HOMO 준위가 전자가 부족한 상태가 되고, 상대적으로 전자가

많은 그래핀으로부터 전자 전달이 일어났다고 여겨진다. 더 나아가, 분자 위에 그래핀을 전사하였을 때에는 광환원 반응이 줄어들었음을 확인하였는데 DR1의 광환원 반응에서 주변에 존재하는 수소가 반응에 영향을 미치는 것으로 여겨진다.

3 장에서는 그래핀의 표면을 passivation 함으로써 그래핀 기반 DNA 센서의 민감도 및 선택도 향상 연구를 소개한다. 산화 그래핀 (Graphene oxide)은 단일 나선 DNA와 이중 나선 DNA에 대해 서로 다른 결합 친화력을 가지며, 형광을 소광시키는 특성을 지니기 때문에 DNA 센서 연구에 활발히 이용되고 있다. 산화 그래핀 표면에 형광 표지된 DNA가 흡착되면 형광이 소광되고 상보적인 DNA를 넣어줌으로 인하여 DNA 이중 나선이 형성된다. 형성된 이중 나선 DNA은 그래핀과 결합 친화력이 비교적 떨어지기 때문에 그래핀 표면으로부터 분리되고 형광이 다시 나타나게 된다. 그러나 실제 실험에서 산화 그래핀의 표면이 탐침 DNA로 완전히 덮여 있지 않고 따라서 넣어준 상보적 DNA (cDNA) 또는 비상보적 DNA (mDNA)들이 바로 탐침 DNA와 상호 작용하지 않고 그래핀 표면에 비특이적으로 결합하는 경우가 종종 관찰된다. 이러한 원하지 않는 결합은 형광 변화를 약화시키기 때문에 센서의 감도 민감성과 선택성을 상당히 저하시킨다. 따라서, 비어있는 산화 그래핀 표면을 passivation 시킨 그래핀 기반 DNA 센서는 기존 센서들에 비해 향상된 성능을 가진다.

주요어: 그래핀, 그래핀 표면 증강 분광법, 그래핀 샌드위치 구조, 양자 공극 공간, 광촉매, 형광 소광, DNA 센서

학번: 2013-22932